

# Modelling Uncertainty in Representation of Facial Features for Face Recognition

Hiremath P.S., Ajit Danti and Prabhakar C.J.  
*Gulbarga University, Gulbarga; JNN College of Engineering, Shimoga & Kuvempu University, Shimoga  
India*

## 1. Introduction

Face is one of the important biometric identifier used for human recognition. The face recognition involves the computation of similarity between face images belonging to the determination of the identity of the face. The accurate recognition of face images is essential for the applications including credit card authentication, passport identification, internet security, criminal databases, biometric cryptosystems etc. Due to the increasing need for the surveillance and security related applications in access control, law enforcement, and information safety due to criminal activities, the research interest in the face recognition has grown considerably in the domain of the pattern recognition and image analysis. A number of approaches for face recognition have been proposed in the literature (Zhao et al. 2000), (Chellappa et al. 1995). Many researchers have addressed face recognition based on geometrical features and template matching (Brunelli and Poggio, 1993). There are several well known face recognition methods such as Eigenfaces (Turk and Pentland 1991), Fisherfaces (Belhumeur et al. 1997), (Kim and Kitter 2005), Laplacianfaces (He et al. 2005). The wavelet based Gabor function provide a favorable trade off between spatial resolution and frequency resolution (Gabor 1946). Gabor wavelets render superior representation for face recognition (Zhang, et al. 2005), (Shan, et al. 2004), (Olugbenga and Yang 2002).

In recent survey, various potential problems and challenges in the face detection are explored (Yang, M.H., et al., 2002). Recent face detection methods based on data-driven learning techniques, such as the statistical modeling methods (Moghaddam and Pentland 1997), (Schneiderman, and Kanade, 2000), (Shih and Liu 2004), the statistical learning theory and SVM based methods (Mohan et al., 2001). Schneiderman and Kanade have developed the first algorithm that can reliably detect human faces with out-of-plane rotation and the first algorithm that can reliably detect passenger cars over a wide range of viewpoints (Schneiderman and Kanade 2000). The segmentation of potential face region in a digital image is a prelude to the face detection, since the search for the facial features is confined to the segmented face region. Several approaches have been used so far for the detection of face regions using skin color information. In (Wu, H.Q., et al., 1999), a face is detected using a fuzzy pattern matching method based on skin and hair color. This method has high detection rate, but it fails if the hair is not black and the face region is not elliptic. A face detection algorithm for color images using a skin-tone color model and facial features is

presented in (Hsu et al. 2002). Face recognition can be defined as the identification of individuals from images of their faces by using a stored database of faces labeled with people's identities. This task is complex and can be decomposed into the smaller steps of detection of faces in a cluttered background, localization of these faces followed by extraction of features from the face regions, and finally, recognition and verification. It is a difficult problem as there are numerous factors such as 3D pose, facial expression, hair style, make up etc., which affect the appearance of an individual's facial features. In addition to these facial variations, the lighting, background, and scale changes also make this task even more challenging. Additional problematic conditions include noise, occlusion, and many other possible factors.

Many methods have been proposed for face recognition within the last two decades. Among all the techniques, the appearance-based methods are very popular because of their efficiency in handling these problems (Chellappa et. al. 1995). In particular, the linear appearance based face recognition method known as eigenfaces (Turk & Pentland 1991) is based on the principal component analysis of facial image ensembles (Kirbi & Sirovich 1990). The defining characteristic of appearance-based algorithms is that they directly use the pixel intensity values in a face image as the features on which to base the recognition decision. The pixel intensities that are used as features are represented using single valued variables. However, in many situations same face is captured in different orientation, lighting, expression and background, which lead to image variations. The pixel intensities do change because of image variations. The use of single valued variables may not be able to capture the variation of feature values of the images of the same subject. In such a case, we need to consider the symbolic data analysis (SDA) (Bock & Diday 2000; Diday 1993), in which the interval-valued data are analyzed. Therefore, there is a need to focus the research efforts towards extracting features, which are robust to variations due to illumination, orientation and facial expression changes by representing the face images as symbolic objects of interval type variables (Hiremath & Prabhakar 2005). The representation of face images as symbolic objects (symbolic faces) accounts for image variations of human faces under different lighting conditions, orientation and facial expression. It also drastically reduces the dimension of the image space. In (Hiremath & Prabhakar 2005), a symbolic PCA approach for face recognition is presented, in which symbolic PCA is employed to compute a set of subspace basis vectors for symbolic faces and then project the symbolic faces into the compressed subspace. This method requires less number of features to achieve the same recognition rate as compared to eigenface method. The symbolic PCA technique, however, encodes only for second order statistics, i.e., pixel wise covariance among the pixels, and is insensitive to the dependencies of multiple (more than two) pixels in the patterns. As these second order statistics provide only partial information on the statistics of both natural images and human faces, it might become necessary to incorporate higher order statistics as well. The kernel PCA (Scholkopf et. al. 1998) is capable of deriving low dimensional features that incorporate higher order statistics. Higher order dependencies in an image include nonlinear relations among the pixel intensity values, such as the relationships among three or more pixels in an edge or a curve, which can capture important information for recognition. The kernel PCA is extended to symbolic data analysis as symbolic kernel PCA (Hiremath & Prabhakar 2006) for face recognition and the experimental results show improved recognition rate as compared to the symbolic PCA method. The extension of symbolic analysis to face recognition techniques using methods based on linear discriminant

analysis, two-dimensional discriminant analysis, Independent component analysis, factorial discriminant analysis and kernel discriminant analysis has been attempted in (Hiremath and Prabhakar Dec 2006, Jan 2006, Aug 2006, Sept 2006, 2007).

It is quite obvious that the literature on face recognition is replete with a wide spectrum of methods addressing a broad range of issues of face detection and recognition. However, the objective of the study in the present chapter is the modeling of uncertainty in the representation of facial features, typically arising due to the variations in the conditions under which face images of a person are captured as well as the variations in the personal information such as age, race, sex, expression or mood of the person at the time of capturing the face image. Two approaches, namely, fuzzy-geometric approach and symbolic data analysis, for face recognition are considered for the modeling of uncertainty of information about facial features.

## **2. Fuzzy face Mode for Face Detection**

In (Hiremath and Danti, Dec 2005), the detection of the multiple frontal human faces based on the facial feature extraction, using the fuzzy face model and the fuzzy rules, is proposed and it is described in this section. The input color image is searched for the possible skin regions using the skin color segmentation method. In which, 2D chromatic space CbCr using the sigma control limits on the chromatic components Cb and Cr, derived by applying the statistical sampling technique. Each potential face region is then verified for a face in which, initially, the eyes are searched and then the fuzzy face model is constructed by dividing the human facial area into quadrants by two reference lines drawn with respect to the eyes. Further, other facial features such as mouth, nose and eyebrows are searched in the fuzzy face model using the fuzzy rules and then face is detected by the process of defuzzification. Overview of this fuzzy-geometric approach is shown in the Figure 3.

### **2.1 Skin Color Segmentation**

Face detection based on skin color is invariant of facial expressions, rotations, scaling and translation (Hsu et al. 2002). Human skin color, with the exception of very black complexion, is found in a relatively narrow color space. Taking advantage of this knowledge, skin regions are segmented using the skin color space as follows.

#### **Skin Color Space**

The YCbCr color model is used to build the skin color space. It includes all possible skin colors. We are able to extract more facial skin color regions excluding the non-skin regions. The skin color space uses only the chromatic color components Cb and Cr for skin color segmentation using the sigma control limits (Hiremath and Danti, Feb 2006). The procedure to build skin color space is described as following.

The sample images are in RGB colors. The RGB color space represents colors with luminance information. Luminance varies from person to person due to different lighting conditions and hence luminance is not a good measure in segmenting the human skin color. The RGB image is converted into YCbCr color model in which luminance is partially separated (Jain A.K. 2001). Skin color space is developed by considering the large sample of facial skins cropped manually from the color face images of the multi racial people. Skin samples are then filtered using low pass filter (Jain 2001) to remove noises. The lower and

upper control limits of the pixel values for the chromatic red and blue color components are determined based on one-and-half sigma limits using the equation (1).

$$\mu_i = \frac{1}{(m \times n)} \sum_{x=1}^m \sum_{y=1}^n c(x,y), \quad \bar{\mu} = \frac{1}{k} \sum_{i=1}^k \mu_i, \quad \sigma = \sqrt{\frac{\sum_{i=1}^k (\mu_i - \bar{\mu})^2}{k}} \quad (1)$$

$$lcl = \bar{\mu} - 1.5\sigma, \quad ucl = \bar{\mu} + 1.5\sigma$$

where  $\mu_i$  denote the mean of the chromatic color components of the  $i^{th}$  sample image  $c(x,y)$  of size  $m \times n$ , where  $c$  denotes the color plane (i.e. red and blue).  $\bar{\mu}$  and  $\sigma$  denotes mean and standard deviation of the color components of the population of all the  $k$  sample images respectively. The lower and upper control limits,  $lcl$  and  $ucl$  of the chromatic color components of skin color, respectively, are used as threshold values for the segmentation of skin pixels as given below

$$P(x,y) = \begin{cases} 1, & \text{if } (lcl_r \leq Cr(x,y) \leq ucl_r) \ \& \ (lcl_b \leq Cb(x,y) \leq ucl_b), \\ 0, & \text{Otherwise,} \end{cases} \quad (2)$$

where  $Cr(x,y)$  and  $Cb(x,y)$  are the chromatic red and blue component values of the pixel at  $(x,y)$  in the red and blue planes of the test image respectively. Hence, the lower and upper sigma control limits  $lcl_r$  and  $ucl_r$  for red and  $lcl_b$  and  $ucl_b$  for blue colors, can transform a color image into a binary skin image  $P$ , such that the white pixels belong to the skin regions and the black pixels belong to the non skin region as shown in the Figure 1(b). In the computation of the lower and upper control limits, experimental results show that, in the  $3\sigma$  limits, the probability of inclusion of non-skin pixels in the face area is high. On the contrary, in the  $\sigma$  limits, the probability of omission of facial skin pixels in the face area is high. It is found that  $1.5\sigma$  limits are the optimal limits, which yield a suitable trade off between the inclusion of facial skin pixels and the omission of non-skin pixels in the face area. In the experiments, the values of the mean  $\bar{\mu}$  and the standard deviation  $\sigma$ , and lower and upper control limits of the chromatic color components are quantified based on the several sample skin images of the multiracial people and are mentioned in the Table 1. The sigma control limits are flexible enough to absorb the moderate variations of lighting conditions in the image to some extent. The results of the skin color segmentation are shown in the Figure 1(b). The skin color segmentation leads to a faster face detection process as the search area for the facial features is comparatively less. The comparative analysis of the different skin color segmentation methods is shown in the Table 2.

Color Component	Mean ( $\bar{\mu}$ )	Std. Dev. ( $\sigma$ )	$lcl$	$ucl$
Cb (Blue)	120	15	97.5	142.5
Cr (Red)	155	14	134	176

Table 1. Statistical values for the skin color space

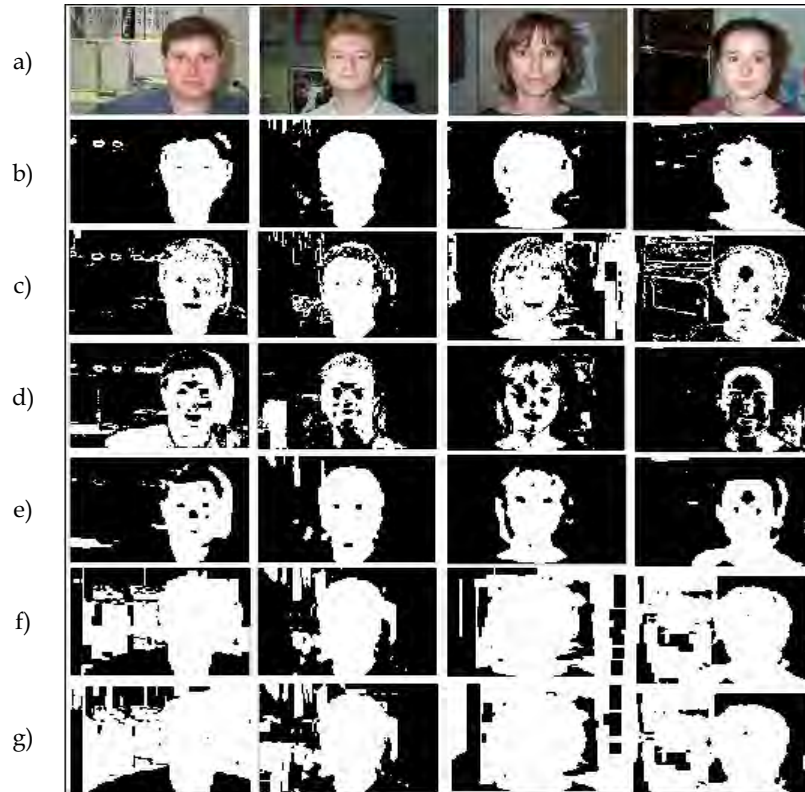


Figure 1. Comparison of skin segmentation results. a) Original Image, b) YCbCr (Hiremath-Danti, Feb 2006), c) RGB (Wang-Yuan method), d) HSV (Bojic method), e) YCbCr (Chai method), f) YUV (Yao method), g) YIQ (Yao method)

Skin Color spaces based on	Avg. time (In secs)	Std. Dev.	% Avg segmented skin area	Avg No. of facial feature blocks
RGB Model (Wang & Yuan 2001)	1.04	0.0332	29.00	67
HSV Model (Bojic & Pang 2000)	0.59	0.0395	32.83	84
YCbCr Model (Chai & Ngan 1999)	2.12	0.0145	26.31	26
YUV Model (Yao and Gao 2001)	1.01	0.0136	52.85	99
YIQ Model (Yao and Gao 2001)	1.05	0.0143	66.07	105
YCbCr (Hiremath & Danti, Feb 2006)	0.82	0.0137	25.28	21

Table 2. Comparison of time, segmented skin area, and number of candidate facial feature blocks for the various skin color segmentation methods

#### Pre processing of Skin Segmented Image

The binary skin segmented image obtained above is preprocessed by performing binary morphological opening operation to remove isolated noisy pixels. Further, white regions

may contain black holes these black holes may be of any size and are filled completely. The binary skin image is labeled using the region labeling algorithm and their feature moments, such as center of mass  $(\bar{x}, \bar{y})$ , orientation  $\theta$ , major axis length, minor axis length and area, are computed (Jain, A.K., 2001; Gonzalez, R.C., et al., 2002). By the observation of several face regions under analysis, it is found that the face regions are oriented in the range of  $\pm 45^\circ$  degrees in the case of frontal view of the face images. Only such regions are retained in the binary skin image for further consideration. The remaining regions are considered as non face regions and are removed from the binary skin image. The observation of several real faces also revealed that the ratio of height to width of each face region is approximately 2, only such regions are retained. Further, though the skin regions of different sizes are successfully segmented, it is found that the potential facial features are miss-detected whenever the face area is less than 500 pixels. Hence, the regions, whose area is more than the 500 pixels are considered for the face detection process. The resulting binary skin image after the preprocessing and applying the above constraints is expected to contain potential face regions (Fig 2(a), (b)).



Figure 2. Results of Skin color segmentation a) Original Image b) Potential face regions in gray scale image c) Sobel Filtered Binary image

## 2.2 Face Detection

Each potential face region in the binary image is converted into gray scale image as shown in Figure 2.(b) and then each face region is passed on to our fuzzy face model to decide whether the face is present in that region or not, by the process of facial feature extraction using the fuzzy rules (Hiremath & Danti Dec. 2005). The detailed face detection process, which detects multiple faces in an input image, is described in Figure 3.

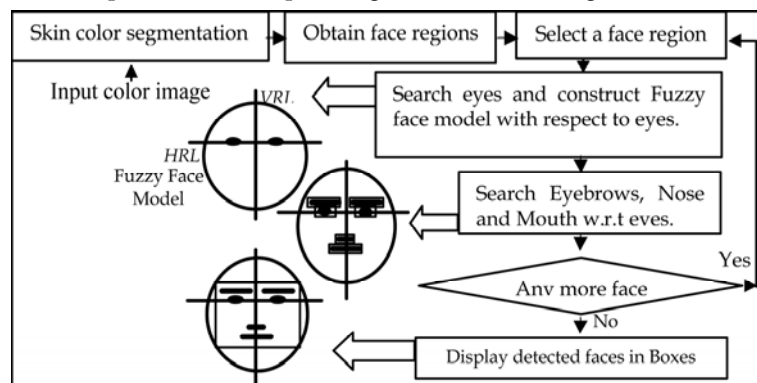


Figure 3. Overview of the multiple face detection process

### Preprocessing of Face Regions

The each gray scale version of the potential face region is filtered using the Sobel edge filter and binarized using a simple global thresholding and then labeled. In the labeled image, the essential facial feature blocks are clearly visible in the potential face region under consideration Figure 2(c). Further, for each facial feature block, its center of mass  $(\bar{x}, \bar{y})$ , orientation  $\theta$ , bounding rectangle and the length of semi major axis are computed (Jain, A.K., 2001).

### Feature Extraction

The feature blocks of the potential face region in the labeled image are evaluated in order to determine which combination of feature blocks is a potential face and the procedure is explained as follows:

#### Searching Eyes

The eyes are detected by exploiting the geometrical configuration of the human face. All the feature blocks are evaluated for eyes. Initially, any two feature blocks are selected arbitrarily and assume them as probable eye candidates. Let  $(x_1, y_1)$  and  $(x_2, y_2)$  be respectively, the centers of right feature block and left feature block. The line passing through the center of both the feature blocks is called as the *horizontal-reference-line (HRL)* as shown in Figure 4 and is given by the equation (3) and the slope angle  $\theta_{HRL}$  between the HRL and x-axis is given by equation (4).

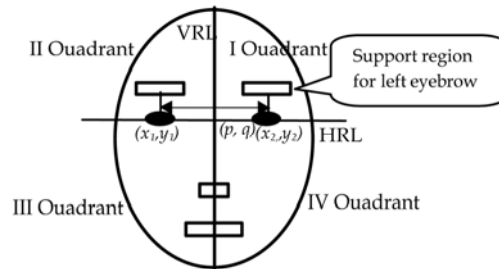


Figure 4. Fuzzy face model with support regions for eyebrows, nose and mouth shown in rectangles

$$ax + by + c_{HRL} = 0$$

$$\text{where, } a = y_2 - y_1, \quad b = x_1 - x_2, \quad c_{HRL} = x_2 y_1 - x_1 y_2 \quad (3)$$

The slope angle  $\theta_{HRL}$  between the HRL and x-axis is given by:

$$\theta_{HRL} = \tan^{-1}(-a/b), \quad -\pi/2 \leq \theta_{HRL} \leq \pi/2 \quad (4)$$

Since the fuzzy face model is a frontal view model, a face in a too skewed orientation is not considered in this model. Hence, the slope angle  $\theta_{HRL}$  is constrained within the range of  $\pm 45^\circ$ . If the current pair of feature blocks does not satisfy this orientation constraint, then they are rejected and another pair of feature blocks from the remaining feature blocks is taken for matching. Only for the accepted pairs of features, the normalized lengths of the semi major axis  $l_1$  and  $l_2$  are computed by dividing the length of the semi major axis by the distance D between these two features. The distance D is given by the equation (5).

$$D = \left[ (x_1 - x_2)^2 + (y_1 - y_2)^2 \right]^{1/2} \quad (5)$$

Let  $\theta_1$  and  $\theta_2$  are the orientations of the above accepted feature blocks. The evaluation function  $E_{Eye}$  is computed using the equation (6) to check whether the current pair of features is a potential eye pair or not.

$$E_{Eye} = \exp \left[ -1.2 \left( (l_1 - l_2)^2 + (l_1 + l_2 - 1)^2 + (\theta_1 - \theta_{HRL})^2 + (\theta_2 - \theta_{HRL})^2 \right) \right] \quad (6)$$

This evaluation function value ranges from 0 to 1 and it can be given the interpretation of a probability value. The constant 1.2 is the mean of the negative exponential distribution, which is determined empirically with respect to the sample images considered for experimentation to optimize higher detection rate with lower false detections. Hence, higher the evaluation value  $E_{Eye}$  higher is the probability of the two selected feature blocks to be eyes. If this evaluation value is greater than an empirical threshold value 0.7, then these two feature blocks are accepted as the *potential eye pair candidate*. Otherwise, this pair of blocks is rejected and another pair of feature blocks is selected. For potential eye pair candidate, the fuzzy face model is constructed and the other facial features are searched as follows.

#### Construction of Fuzzy Face Model

It is assumed that every human face is having the same geometrical configuration and the relative distances between the facial features are less sensitive to poses and expressions (Yang et al. 2002). The fuzzy face model is constructed with respect to the above potential eye candidates. A line perpendicular to the *HRL* at the mid point of the two eyes is called as vertical reference line (*VRL*). Let  $(p, q)$  be the mid point of the line segment joining the centers of the two eye candidates. Then the equation of the *VRL* is given by equation (7).

$$bx - ay + c_{VRL} = 0 \quad (7)$$

These two reference lines (*HRL* and *VRL*) are used to partition the facial area into quadrants as shown in Figure 4. The vertical and horizontal distances of the facial features namely, eyebrows, nose and mouth are empirically estimated in terms of the distance  $D$  between the centers of the two eyes on the basis of the observations from several face images. The notations  $V_{Eyebrows}$ ,  $V_{Nose}$  and  $V_{Mouth}$  denote the vertical distances of the centers of eyebrows, nose and mouth from the *HRL* which are estimated as  $0.3D$ ,  $0.6D$  and  $1.0D$  respectively. The notations  $H_{Eyebrows}$ ,  $H_{Nose}$  and  $H_{Mouth}$  denote the horizontal distances of the centers of eyebrows, nose and mouth from the *VRL* which are estimated as  $0.5D$ ,  $0.05D$  and  $0.1D$  respectively. The facial features are enclosed by the rectangles to represent the support regions, which confine the search area for facial features. This completes the construction of the fuzzy face model with respect to the selected potential eye pair candidate in the given face region as shown in Figure 4. Further, the fuzzy face model is used to determine which combination of the feature blocks is a face.

#### Searching Eyebrows, Nose and Mouth

The searching process proceeds to locate the other potential facial features, namely eyebrows, nose and mouth with respect to the above potential eye pair candidate. The support regions for eyebrows, nose and mouth are empirically determined using fuzzy rules as given in Table 3. Then these support regions are searched for facial features. For illustration, we take the left eyebrow feature as an example to search. Let a feature block  $K$

be a potential left eyebrow feature. The horizontal distance  $h_{Leb}$  and the vertical distance  $v_{Leb}$  of the centroid of the  $K^{th}$  feature from the VRL and HRL, respectively, are computed using the equation (8).

Feature(j)	Vertical distances				Horizontal distances			
	$\min_{v_j}$	$\max_{v_j}$	$\bar{v}_j$	$\sigma_{v_j}$	$\min_{h_j}$	$\max_{h_j}$	$\bar{h}_j$	$\sigma_{h_j}$
Eyebrows	0.02	0.38	0.2	0.06	0.24	0.65	0.45	0.07
Nose	0.30	0.90	0.6	0.10	-0.2	0.2	0.0	0.07
Mouth	0.45	1.35	0.9	0.15	-0.3	0.3	0.0	0.10

Table 3. Empirically determined distances of the facial features (normalized by D)

$$h_{Leb} = \frac{|b\bar{x}_K - a\bar{y}_K + c_{VRL}|}{(a^2 + b^2)^{1/2}} \quad \text{and} \quad v_{Leb} = \frac{|a\bar{x}_K + b\bar{y}_K + c_{HRL}|}{(a^2 + b^2)^{1/2}}, \quad (8)$$

Treating  $h_{Leb}$  and  $v_{Leb}$  as the fuzzy quantities to represent the possible location of the potential left eyebrow feature, the fuzzy membership values  $\mu_{h_{Leb}}$  and  $\mu_{v_{Leb}}$ , respectively, are defined using the trapezoidal fuzzy membership function (Hines & Douglas 1990). In particular, the membership function  $\mu_{v_{Leb}}$  is defined using the equation (9) and Table 3.

$$\mu_{v_{Leb}}(v_{Leb}) = \begin{cases} 0, & \text{if } v_{Leb} \leq \min v_{Leb} \\ \frac{(v_{Leb} - \min v_{Leb})}{(\alpha - \min v_{Leb})}, & \text{if } (\min v_{Leb} \leq v_{Leb} \leq \alpha) \\ 1, & \text{if } (\alpha \leq v_{Leb} \leq \beta) \\ \frac{(\max v_{Leb} - v_{Leb})}{(\max v_{Leb} - \beta)}, & \text{if } (\beta \leq v_{Leb} \leq \max v_{Leb}) \\ 0, & \text{if } (v_{Leb} \geq \max v_{Leb}) \end{cases} \quad (9)$$

Similarly, the membership function  $\mu_{h_{Leb}}$  is defined. The support region for the potential left eyebrow feature is the set of values  $h_{Leb}$  and  $v_{Leb}$  whose fuzzy membership values are non-zero. The Figure 5(a) shows the graph of the trapezoidal fuzzy membership function  $\mu_{v_j}$  for the vertical distance of the  $j^{th}$  feature and the support region for the left eyebrow is shown in Figure 5(b). To evaluate  $K^{th}$  feature block in the support region for left eyebrow, the value of the evaluation function  $E_K$  is given by the equation (10). The  $E_K$  value ranges from 0 to 1 and represents the probability that the feature block  $K$  is a left eyebrow.

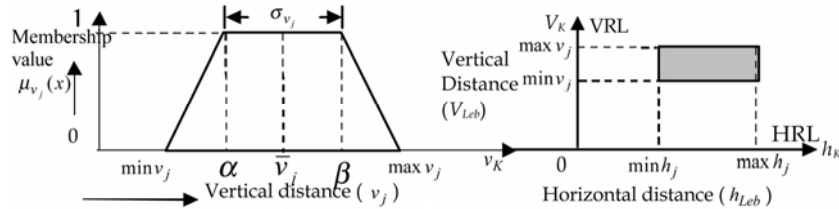


Figure 5. Trapezoidal fuzzy membership function  $\mu_{v_j}$  for the vertical distance of the  $j^{th}$  facial feature b) Support region for left eyebrow in the I quadrant of face model

$$E_K = \frac{1}{2} \left( \exp \left[ -1.2 \left( \frac{v_{Leb} - V_{Eyebrows}}{D/2} \right)^2 \right] + \exp \left[ -1.2 \left( \frac{h_{Leb} - H_{Eyebrows}}{D/2} \right)^2 \right] \right) \quad (10)$$

Similarly, evaluation value is computed for all the feature blocks present in that support region of the left eyebrow. The evaluation value  $E_{Leb}$  is a fuzzy quantity represented by the set of  $E_K$  values with their corresponding fuzzy membership values  $\mu_K$ . The membership value  $\mu_{Leb}$  corresponding to  $E_{Leb}$  is obtained by the *min-max* fuzzy composition rule (Klir & Yuan 2000) given by the equations (11) and (12). The feature block having the evaluation value  $E_{Leb}$  with the corresponding  $\mu_{Leb}$  found in the support region of the left eyebrow is the *potential left eyebrow* feature with respect to the current pair of potential eye candidates.

$$\mu_K = \min(\mu_{h_K}, \mu_{v_K}), \text{ for each } K \quad (11)$$

$$\mu_{Leb} = \max_K \{\mu_K\} \quad (12)$$

Similarly, the right eyebrow, nose and mouth are searched in their respective support regions determined by appropriately defining the membership functions for the fuzzy distances (horizontal and vertical) from the centroid of these facial features, and their fuzzy evaluation values are computed by applying the *min-max* fuzzy composition rule. The overall fuzzy evaluation  $E$  for the fuzzy face model is defined as the weighted sum of the fuzzy evaluation values of the potential facial features namely, for the eye, left eyebrow, right eyebrow, nose and mouth, respectively. The weights are adjusted to sum to unity as given in the equation (13). The membership value  $\mu_E$  corresponding to  $E$  is obtained by the fuzzy composition rule as given by the equation (14).

$$E = 0.4E_{Eye} + 0.3E_{Mouth} + 0.2E_{Nose} + 0.05E_{Leb} + 0.05E_{Reb} \quad (13)$$

$$\mu_E = \min\{\mu_{Mouth}, \mu_{Nose}, \mu_{Leb}, \mu_{Reb}\} \quad (14)$$

Above procedure is repeated for every potential eye pair candidate and get the set of fuzzy faces. These fuzzy faces are represented by the set of  $E$  values with their corresponding membership values  $\mu_E$ . Finally, the most probable face is obtained by the defuzzification process as given by the equation (15).

$$\mu_{E_{max}} = \max_{E \in \Omega} \{\mu_E\} \quad (15)$$

Then the  $E$  value corresponding to  $\mu_{E_{max}}$  is the defuzzified evaluation value  $E_D$  of the face. If there are more than one  $E$  value corresponding to  $\mu_{E_{max}}$ , the maximum among those values is the defuzzified evaluation value  $E_D$  of the face. Finally, the potential eyes, eyebrows, nose and mouth features corresponding to the overall evaluation value  $E_D$  constitute the most probable face in the given face region, provided  $E_D$  is greater than the empirical threshold value 0.7. Otherwise this face region is rejected. The face detection results are shown in Figure 6, where (a) display the feature extraction in which facial features are shown in bounding boxes (Jain 2001) and (b) shows detected face in rectangular box. (Hiremath P.S. & Danti A. Feb 2006). The above procedure is repeated for every potential face region to detect possible faces in the input image.



Figure 6. Results of Face Detection a) Facial Feature extraction b) Detected face in box

### 2.3 Experimental Results

The MATLAB 6.0 implementation of the above described procedure on Pentium IV @ 2.6 GHz yields the success rate of 96.16%. The average time taken to detect one face is about 0.78 sec, which depends on the size of the potential face region. The search area for the facial feature extraction is confined to only the total area covered by the support regions i.e.  $0.67D^2$ , ( $D$  is distance between eyes) which is considerably very small compared to that of the image size. This reduced search area leads to the reduction in the detection time to a great extent. Sample detection results are shown in Figure 7 and Figure 8 with detected faces enclosed in rectangular boxes. Due to the constraints of the face model, miss-detection occurs due to several reasons i.e. profile (side) view faces, abnormal lighting conditions, face occluded by hair, very small face sizes, face occluded by hand and too dark shadow on faces as shown in Figure 9.

The comparison of different state of the art detectors proposed by (Shih and Liu 2004, we refer as S-L method) and (Schneiderman and Kanade 2000, we refer as S-K method) and (Hiremath and Danti, Dec. 2005, we refer as H-D method) is given in Table 4. It is observed that, fuzzy face model approach based on skin color segmentation (H-D method) is comparable to others in terms of detection rate and very low in both detection time and false detections.

Method	Det. Rate (%)	False detection	Det. Time (secs)	Dataset	No. of images	No. of faces
S-L method	98.2	2	not reported	MIT-CMU	92	282
S-K method	94.4	65	5	MIT-CMU	125	483
H-D method	96.1	02	0.78	CIT, FERET, Internet	650	725

Table 4. Comparison of performance



Figure 7. Sample detection results for single as well as multiple human faces with sizes, poses, expressions and complex backgrounds



Figure 8. Sample images with expressions, lighting conditions, complex background & beards



Figure 9. Sample images with miss-detections

### 3. Optimization of feature sets

A small set of geometrical features is sufficient for the face recognition task, which requires less computational time and less memory due to their low dimension. In this approach, facial features detected based on the Fuzzy face model are considered. The normalized geometrical feature vector is constructed with the distances, areas, evaluation values and fuzzy membership values. Normalization is done with respect to the distance between eyes. Further, the feature vector is optimized and demonstrated that the resultant vector is invariant of scale, rotation, and facial expressions. This vector uniquely characterizes each human face despite changes in rotation, scale and facial expressions. Hence, it can be effectively used for the face recognition system. Further, it is a 1-dimensional feature vector space which has reduced dimensionality to a greater extent as compared to the other methods (Turk & Pentland, 1991; Belhumeur et al., 1997) based on the 2-dimensional image intensity space. In (Hiremath and Danti, Dec. 2004), the method of optimization of feature sets for face recognition is presented and it is described as below.

#### 3.1 Geometrical Facial Feature Set

The geometrical facial feature set contains total of about 26 features, in which 12 facial features are obtained from face detector and remaining 14 projected features are determined by the projection of facial features such as eyes, eyebrows, nose, mouth and ears.

##### Facial Features

Using the face detector based on Lines-of-Separability face model (Hiremath P.S. & Danti A., Feb. 2006) and fuzzy face model (Hiremath P.S. & Danti A., Dec. 2005) respectively, the list of geometrical facial features extracted are given in the Table 5.

##### Projected Features

The centroid of the facial features obtained by our face detectors are projected perpendicularly to the *Diagonal Reference Line (DRL)* as shown in the Figure 10. The *DRL* is

the line bisecting the first quadrant in the  $HRL$ - $VRL$  plane and is a locus of point  $(x,y)$  equidistant from  $HRL$  and  $VRL$ . The equation of the  $DRL$  is given by:

$$Ax + By + C = 0, \text{ where the coefficients } A, B, \text{ and } C \text{ are given by:} \quad (16)$$

$$A = (a - b), \quad B = (a + b), \quad C = (c_{HRL} - c_{VRL}) \quad (17)$$

Feature	Description	Feature	Description
$E_{Eyes}$	Evaluation value of eyes	$E_{Rear}$	Evaluation value of right ear
$E_{Leb}$	Evaluation value of left eyebrow	$E$	Overall evaluation value of the face
$E_{Reb}$	Evaluation value of right eyebrow	$\mu_{Leb}$	Membership value of left eyebrow
$E_{Nose}$	Evaluation value of nose	$\mu_{Reb}$	Membership value of right eyebrow
$E_{Mouth}$	Evaluation value of mouth	$\mu_{Nose}$	Membership value of nose
$E_{Lear}$	Evaluation value of left ear	$\mu_{Mouth}$	Membership value of mouth

Table 5. List of geometrical features extracted from face detectors

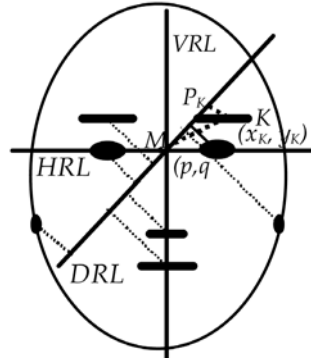


Figure 10. Projection of features onto  $DRL$

#### Distance Ratio Features

The distance ratios are computed as described in the following. Let  $(x_K, y_K)$  be the centroid  $K$  of the  $k^{\text{th}}$  feature (e.g. left eyebrow in the Figure 10). Let  $P_K$  be the projection of point  $K$  on the  $DRL$ . Then, the following distances are computed:

$$KP_K = \left| \frac{Ax_K + By_K + C}{\sqrt{A^2 + B^2}} \right| \quad (\text{Perpendicular distance}) \quad (18)$$

$$MK = \sqrt{(p - x_K)^2 + (q - y_K)^2} \quad (\text{Radial distance}) \quad (19)$$

$$MP_K = \sqrt{MK^2 - KP_K^2} \quad (\text{Diagonal distance}) \quad (20)$$

$$R_{Leb} = \frac{KP_K}{MP_K} \quad (\text{Distance ratio}) \quad (21)$$

The notation,  $R_{Leb}$  denote the distance ratio obtained by the projection of left eyebrow. Similarly the distance ratios  $R_{Le}$ ,  $R_{Re}$ ,  $R_{Reb}$ ,  $R_{Nose}$ ,  $R_{Mouth}$ ,  $R_{Lear}$  and  $R_{Rear}$  are determined, respectively for left eye, right eye, right eyebrow, nose, mouth, left ear and right ear.

#### Distance Ratio Features in Combination

The distances of all the facial features along the DRL are used to compute the distance ratios for the combination of facial features as follows.

$$R_{Leye2Reye} = \frac{MP_{Leye}}{MP_{Reye}} \quad (\text{Left Eye to Right Eye}) \quad (22)$$

$$R_{Leb2Reb} = \frac{MP_{Leb}}{MP_{Reb}} \quad (\text{Left Eyebrow to Right Eyebrow}) \quad (23)$$

$$R_{N2M} = \frac{MP_n}{MP_m} \quad (\text{Nose to Mouth}) \quad (24)$$

$$R_{Lear2Rear} = \frac{MP_{Lear}}{MP_{Rear}} \quad (\text{Left Ear to Right Ear}) \quad (25)$$

#### Area Features

The centroids of the eyes, eyebrows, nose and mouth are connected in triangles as shown in the Figure 11. The areas covered by the triangles are used to determine the area features. In Figure 11(a),  $e_1$  and  $e_2$  denote right and left eyes respectively;  $n$  and  $m$  denote nose and mouth respectively. The coordinates  $(x_1, y_1)$ ,  $(x_2, y_2)$ ,  $(x_3, y_3)$ , and  $(x_4, y_4)$  are the centroids of right eye, left eye, nose, and mouth respectively.

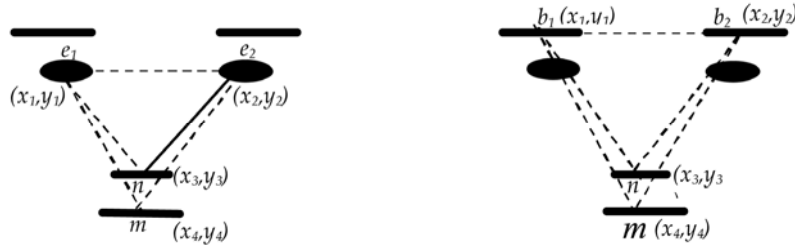


Figure 11. Triangular area features (a) Areas formed by eyes, nose, and mouth (b) Areas formed by eyebrows, nose, and mouth

The triangular area  $A_{en}$  formed by eyes and nose; and, the triangular area  $A_{em}$  formed by eyes and mouth are computed as given below.

$$A_{en} = 0.5 \begin{vmatrix} (x_1 - x_3) & (y_1 - y_3) \\ (x_2 - x_3) & (y_2 - y_3) \end{vmatrix} \quad \&\& \quad A_{em} = 0.5 \begin{vmatrix} (x_1 - x_4) & (y_1 - y_4) \\ (x_2 - x_4) & (y_2 - y_4) \end{vmatrix} \quad (26)$$

$$A_{Eyes} = \frac{A_{en}}{A_{em}} \quad (27)$$

Then the ratio of areas covered by eyes, nose and mouth is given by the equation (27). Similarly, in Figure 11(b),  $b_1$  and  $b_2$  denote right and left eyebrows respectively, and  $n$  and  $m$  denote nose and mouth respectively. The coordinates  $(x_1, y_1)$ ,  $(x_2, y_2)$ ,  $(x_3, y_3)$ , and  $(x_4, y_4)$  are the centroids of right eyebrow, left eyebrow, nose, and mouth respectively. The triangular area  $A_{ebn}$  formed by eyebrows and nose; and, the triangular area  $A_{ebm}$  formed by eyebrows and mouth are computed as given below.

$$A_{ebn} = 0.5 \begin{vmatrix} (x_1 - x_3)(y_1 - y_3) \\ (x_2 - x_3)(y_2 - y_3) \end{vmatrix} \quad \& \quad A_{ebm} = 0.5 \begin{vmatrix} (x_1 - x_4)(y_1 - y_4) \\ (x_2 - x_4)(y_2 - y_4) \end{vmatrix} \quad (28)$$

$$A_{Eyebrows} = \frac{A_{ebn}}{A_{ebm}} \quad (29)$$

Then the ratio of areas covered by eyebrows, nose and mouth is given by the equation (29). The projected features are listed in the Table 6.

Feature	Description	Feature	Description
$R_{Leye}$	Distance ratio by left eye	$R_{Rear}$	Distance ratio by right ear
$R_{Reye}$	Distance ratio by right eye	$R_{Leye2Reye}$	Distance ratio by left and right eyes
$R_{Leb}$	Distance ratio by left eyebrow	$R_{Reb2Leb}$	Distance ratio by left & right eyebrows
$R_{Reb}$	Distance ratio by right eyebrow	$R_{N2M}$	Distance ratio by nose and mouth
$R_{Nose}$	Distance ratio by nose	$R_{Lear2Rear}$	Distance ratio by left ear and right ear
$R_{Mouth}$	Distance ratio by mouth	$A_{Eyes}$	Area ratio by eyes, nose and mouth
$R_{Lear}$	Distance ratio by left ear	$A_{Eyebrows}$	Area ratio by eyebrows, nose and mouth

Table 6. List of projected features

Final geometrical features include 26 features, in which 12 features are from the Table 5 and 14 features are from the Table 6.

### 3.2 Optimization of Features Sets

Three subsets of features from 26 features in different combinations are considered for optimization. The subset A, B, C consist of 14, 6, 14 features, respectively as given below.

$$Subset A = (R_{Leye}, R_{Reye}, R_{Leb}, R_{Reb}, R_{Nose}, R_{Mouth}, R_{Lear}, R_{Rear}, R_{Leye2Reye}, R_{Reb2Leb}, R_{N2M}, R_{Lear2Rear}, A_{Eyes}, A_{Eyebrows}) \quad (30)$$

$$Subset B = (E_{Eyes}, E, R_{Reb2Leb}, R_{N2M}, A_{Eyes}, A_{Eyebrows}) \quad (31)$$

$$Subset C = (\mu_{Leb}, \mu_{Reb}, \mu_{Nose}, \mu_{Mouth}, E_{Eyes}, E_{Leb}, E_{Reb}, E_{Nose}, E_{Mouth}, E, R_{Reb2Leb}, R_{Mouth2Nose}, A_{Eyes}, A_{Eyebrows}) \quad (32)$$

The every feature subset is optimized by the maximal distances between the classes and minimal distances between the patterns of one class. Here each class represents one person

and the different images of one person were considered as patterns. The effectiveness of every feature subset is determined by the evaluation function  $F$  as given below.

$$F = \frac{D_d}{D_m} = \frac{\sqrt{\sum_{i=1}^k (M_d - D_i)^2}}{\sqrt{\sum_{i=1}^k (M_m - M_i)^2}} \text{ where } M_i = \frac{\sum_{j=1}^n f_{ij}}{n}, M_m = \frac{\sum_{i=1}^k M_i}{k}, D_m = \sqrt{\frac{\sum_{i=1}^k (M_m - M_i)^2}{k-1}}$$

$$D_i = \sqrt{\frac{\sum_{j=1}^n (M_i - f_{ij})^2}{n-1}}, M_d = \frac{\sum_{i=1}^k D_i}{k}, D_d = \sqrt{\frac{\sum_{i=1}^k (M_d - D_i)^2}{k-1}} \quad (33)$$

where  $M_i$  and  $D_i$  are mean and variance of the feature values  $f_{ij}$  for ( $j=1$  to  $k$ )  $k$  images of the  $i$ -th person respectively,  $M_m$  and  $M_d$  are mean of  $M_i$  and  $D_i$  respectively. The  $F$  value is the ratio of the measures of dispersion of sample standard deviations and of the sample means of the feature values in the  $k$  sample images of a class. For illustration we have used ORL face database, which contain 40 subjects or classes and each of 10 variations. The Figure 12 shows the optimization of feature subsets in which  $F$  values along the y-axis are plotted for 40 classes along the x-axis. The lower  $F$  value indicates the stronger invariance property of the feature subset with respect to scale, rotation and facial expressions. In the Figure 12 it shows that the feature subset C is well optimized with the lowest  $F$  values compared to other subsets and, hence it corresponds to a better feature subset.

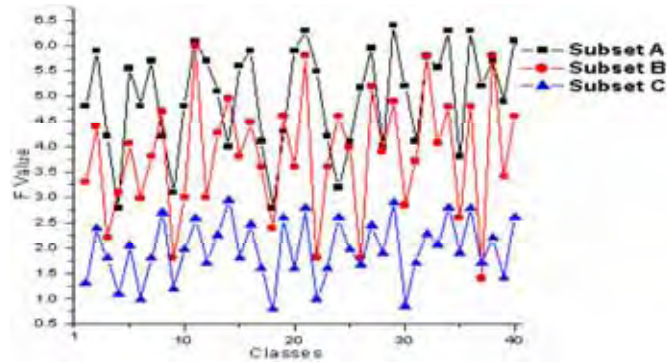


Figure 12. Optimization of subsets of features

### Invariance Property

The above feature Subset C is considered as the most optimized geometrical feature vector for face recognition and is invariant to scaling, rotation, and facial expressions, because the relative geometrical distances between the facial features such as eyes, nose, mouth, and eyebrows vary proportionally with respect to scaling, rotation, and facial expressions, and their feature values remain nearly constant. Hence the optimized feature vector characterizes each human face uniquely. The Figure 13 illustrates the invariance property of

feature vectors for the images shown in Figure 13(a). The Figure 13(b), feature vectors exhibit negligible variations in the feature values.

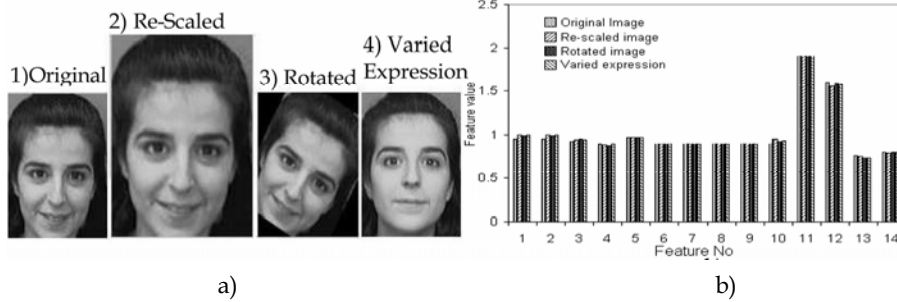


Figure 13. Illustration of invariance property a) Different images of the same person b) Feature vectors for the images in a)

#### 4. Face Recognition

In automated face recognition, a human face can be described by several features, but very few of them are used in combination to improve discrimination ability and different facial features have different contributions in personal identification. The use of geometrical features will always have the credit of reducing huge space that is normally required in face image representation, which in turn increases the recognition speed considerably (Zhao et al. 2000). In (Hiremath and Danti, Jan 2006), the geometric-Gabor features extraction is proposed for face recognition and it is described in this section.

##### 4.1 Gemetric-Gabor feature Extraction

In the human ability of recognizing a face, the local features such as eyes, eyebrows, nose and mouth dominate the face image analysis. In the present study, we have used geometrical features and Gabor features in combination for face recognition. The optimized feature set (Subset C) is considered as *Geometric-Features* for face recognition and the features are listed as below.

$$\begin{aligned} \text{Geometric Features} = & (\mu_{Leb}, \mu_{Reb}, \mu_{Nose}, \mu_{Mouth}, E_{Eyes}, E_{Leb}, E_{Reb}, E_{Nose}, \\ & E_{Mouth}, E, R_{Reb2Leb}, R_{Mouth2Nose}, A_{Eyes}, A_{Eyebrows}) \end{aligned} \quad (34)$$

The Gabor features are extracted by applying the Gabor filters on the facial feature locations as obtained by our face detector and these locations are considered as highly energized points on the face. We refer these Gabor features as *Geometric-Gabor Features* and the feature extraction process is as given below.

The local information around the locations of the facial features is obtained by the Gabor filter responses at the highly energized points on the face. A Gabor filter is a complex sinusoid modulated by a 2D Gaussian function and it can be designed to be highly selective in frequency. The Gabor filters resemble the receptive field profiles of the simple cells in the visual cortex and they have tunable orientation, radial frequency bandwidth and center frequency. The limited localization in space and frequency yields a certain amount of robustness against translation, distortion, rotation and scaling. The Gabor functions are

generalized by Daugman (Daugman 1980) to the following 2D form in order to model the receptive fields of the orientation selective simple cells. The Gabor responses describe a small patch of gray values in an image  $I(x)$  around a given pixel  $x=(x,y)^T$ . It is based on a wavelet transformation, given by the equation:

$$R_i(x) = \int I(x') \psi_i(x-x') dx' \quad (35)$$

This is a convolution of image with a family of Gabor kernels

$$\psi_i(x) = \frac{\|k_i\|^2}{\sigma^2} e^{-\frac{\|k_i\|^2 \|x\|^2}{2\sigma^2}} \left[ e^{jk_i \cdot x} - e^{-\frac{\sigma^2}{2}} \right], \text{ where } k_i = \begin{pmatrix} k_{ix} \\ k_{iy} \end{pmatrix} = \begin{pmatrix} k_v \cos \theta_\mu \\ k_v \sin \theta_\mu \end{pmatrix} \quad (36)$$

Each  $\psi_i$  is a plane wave characterized by the vector  $k_i$  enveloped by a Gaussian function, where  $\sigma$  is the standard deviation of this Gaussian. The center frequency of  $i^{\text{th}}$  filter is given by the characteristic wave vector  $k_i$ , in which scale and orientation given by  $(k_v, \theta_\mu)$ . The first term in the Gabor kernel determines the oscillatory part of the kernel and the second term compensates for the DC value of the kernel. Subtracting the DC response, Gabor filter becomes insensitive to the overall level of illumination. The decomposition of an image into these states is called wavelet transform of the image given by equation (35). Convolution of the input image with complex Gabor filters with 5 spatial frequencies ( $v=0, \dots, 4$ ) and 8 orientations ( $\mu=0, \dots, 7$ ) will capture the whole frequency spectrum, both amplitude and phase, as shown in the Figure 14.

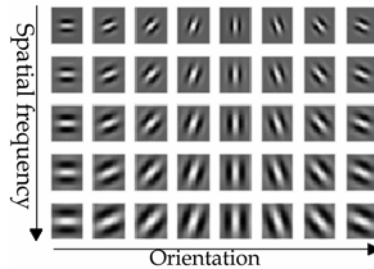


Figure 14. Gabor filters w.r.t. 5 Frequencies and 8 Orientations

In the Figure 15, an input face image (a), the highly energized points (b) and the amplitude of the responses (c) to the above Gabor filters are shown. Several techniques found in the literature for Gabor filter based face recognition consist of obtaining the response at grid points representing the entire facial topology using elastic graph matching for face coding (Kotropoulos et al. April 2000; Wiskott et al.1999; Duc et al. 1999), which generate the high dimensional Gabor feature vector. However, instead of using the graph nodes on entire face, we have utilized only the locations of the facial features such as eyes, eyebrows, nose, and mouth extracted by our face detector (Hiremath P.S. & Danti March 2005) as the highly energized face points (Figure 15(b)) and Gabor filter responses are obtained at these points only. This approach leads to reduced computational complexity and improved performance on account of the low dimensionality of the extended feature vector, which is demonstrated

in the experimental results. Gabor responses are obtained at the highly energized face points of the input face image. A feature point is located at  $(x_0, y_0)$  if

$$R_i(x_0, y_0) = \max_{(x,y) \in W_0} (R_i(x, y)) \text{ and } R_i(x_0, y_0) > \frac{1}{N_1 N_2} \sum_{x=1}^{N_1} \sum_{y=1}^{N_2} R_i(x, y) \quad (37)$$

where  $i=1, \dots, 40$ ,  $R_i$  is the response of the image to the  $i^{\text{th}}$  Gabor filter. The size of the face image is  $N_1 \times N_2$  and the center of the window,  $W_0$ , is at  $(x_0, y_0)$ . The window size  $W$  must be small enough to capture the important features and large enough to avoid redundancy. In our experiments,  $9 \times 9$  window size is used to capture the Gabor responses around the face points. For the given face image, we get 240 Gabor responses (6 highly energized facial feature points and 40 filters) as a Geometric-Gabor feature set. Finally, both the *Geometric-Features* and *Geometric-Gabor-Features* are integrated into an *Extended-Geometric-Feature* vector. These feature vectors are used for the recognition of a face by applying the matching function as described in the next section.

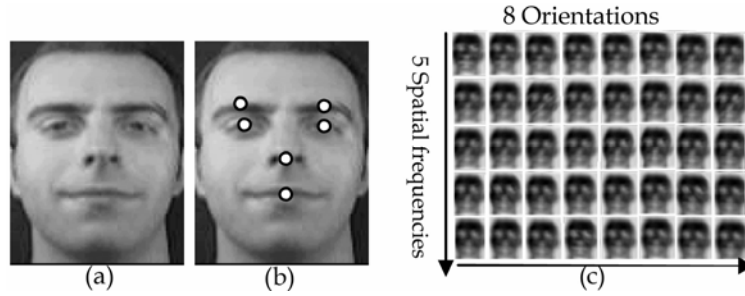


Figure 15. Facial image response to 40 Gabor Filters a) Original Image, b) highly energized face points c) Gabor Filter Responses

#### 4.2 Face Matching

The traditional PCA technique (Turk and Pentland 1991) considers each face image as a feature vector in a high dimensional space by concatenating the rows of the image and using the intensity of each pixel as a single feature. Hence, each image can be represented as an  $n$ -dimensional random vector  $x$ . The dimensionality  $n$  may be very large, of the order of several thousands. The main objective of the PCA is dimensionality reduction, i.e.  $n$ -dimensional vector  $x$  into an  $m$ -dimensional vector, where  $m \ll n$ . A face image is represented by *Geometric-Feature* set and also by *Geometric-Gabor-Feature* set. Further, these two feature sets are integrated into an *Extended-Geometric feature* vector, which is considerably very small compared to that of the feature vector used in (Turk and Pentland 1991). The matching function is evaluated for all the feature sets of the training face images in order to assess the match between the images of the same person (or subject) and the images from different individuals. The match value is determined by comparing a host face with the other face images using the negative exponential function given by:

$$\text{Matching Function} \quad d = \frac{1}{N} \sum_{i=1}^N \exp(-|x_i - y_i|) \quad \text{where } 0 < d < 1 \quad (38)$$

where  $x_i$  and  $y_i$  are the feature elements of the face images  $X$  and  $Y$ , respectively,  $N$  is the total number of elements of the feature. The results of the matching performance for the database faces using the *Geometric-Feature* set, the *Geometric-Gabor-Feature* set and the *Extended-Geometric-Feature* set are shown in the Figure 17(a), (b) and (c), respectively. The match value  $d_{EGF}$  for an *Extended-Geometric-Feature* vector is determined by the average of the match values of Geometric  $d_{GF}$  and Geometric-Gabor  $d_{GGF}$  feature sets as given below:

$$d_{EGF} = \frac{1}{2}[d_{GF} + d_{GGF}] \quad (39)$$

The match values are determined using the matching function. The horizontal axis represents the face number and the vertical axis represents the match between faces for that feature set. The value of the match is within the range  $[0,1]$  and can be given probability interpretation. The match is 1, when the host face is having highest match with that of the target faces and the match is zero, when the host face is having lowest match with that of the target faces. The performance of the features are analyzed by searching for target faces that match with the given host face. The targets are different images of the same person as the host. The analysis is based on the individual assessment of the two feature sets as well as the performance when both the feature sets are integrated into the extended feature vector.

#### 4.3 Experimental Results

For experimentation, the ORL and MIT face databases, which are the publicly available benchmark databases for evaluation, are used. The ORL database consists of 400 images, in which there are 40 subjects (persons) and each having 10 variations i.e. varying expressions, poses, lighting conditions under homogeneous background. The MIT database consists of 432 images, in which there are 16 subjects and each having 27 variations i.e. different head tilts, scales and lighting conditions under moderate background. The experimentation is done with 40 face images, which consist of 10 subjects and each of 4 variations. To illustrate the analysis of experimental results, the Figure 16 depicts face no 21 as host face and face nos. 22, 23 and 24 as its target faces, i.e. these face images pertain to the same subject (person). Results of the match between the face 21 and the other 39 faces are shown in the Figs. 17 (a), (b) and (c) for the *Geometric-Feature* set, the *Geometric-Gabor-Feature* set and the *Extended-Geometric-Feature* vector, respectively. In the Figure 17(a), we observe that some of the non-target faces also yield a comparable match value as that of target faces leading to recognition errors, e.g. non-target face nos. 3, 26 and 27 have match values close to that of target faces no. 23. Further, many of the non-target faces have match values greater than 0.5 leading to the poor discrimination ability of the geometric feature set. Similar observations can be made in the Figure 17(b), but the discrimination ability of Geometric-Gabor feature set is found to be better than the geometric feature set. Only few non-target faces have match values greater than 0.4 and close to the target faces. However, still improved match results are found in case of the integrated feature vector combining geometric as well as Geometric-Gabor features and are depicted in Figure 17(c). All the non-target faces have their match values much less than 0.4 and are well discriminated from the target faces leading to enhanced recognition rate.

The possibility of a good match of the non-target faces on individual feature sets have been reduced and such faces are well discriminated by the integration of both the feature sets as shown in the Figure 17(c). Similar discrimination results are reported when comparing the

effectiveness of template matching to geometric features (Brunelli and Poggio, 1993). In matching, the geometric features remain reasonably constant for a certain extent of variations in face orientation, expressions and tolerate side-to-side rotation better than up-down movement, which are attributed to the normalization by the distance between eyes. However for the geometric features, match fails for upside down faces and extreme illumination conditions, due to the fact that, the fuzzy face model is constrained by the face orientation within the range  $\pm 45^\circ$  and minimum face area of 500 pixels, otherwise the facial features are miss-detected. These factors are greatly affecting the matching performance of the *Geometric-Feature* set. The *Geometric-Gabor-Feature* set performed well on all the faces due to the fact that, Gabor features capture most of the information around the local features, which yields a certain amount of robustness against lighting variations, translation, distortion, rotation and scaling. Further, robustness of Gabor features is also because of capturing the responses only at highly energized fiducial points of the face, rather than the entire image. The Gabor filters are insensitive to the overall level of illumination, but fail for the images under extreme illumination conditions (too darkness). Hence, the match on the *Extended-Geometric-Feature* vector exhibits a balanced performance. Face movement not only affects feature translation and rotation but also causes variation in illumination by changing the position of shadows especially in case of up-down, and side-to-side face movements. Hence this approach is tolerant not just to face movement but also to a certain extent of variations in illumination.

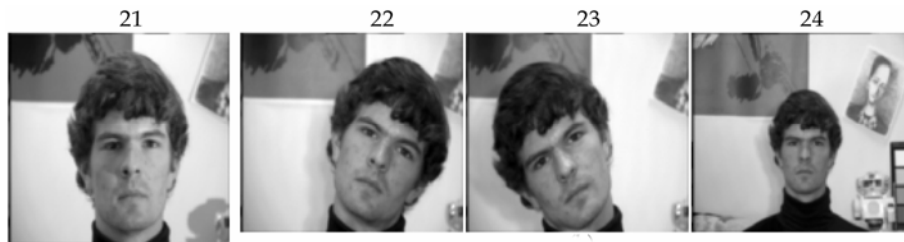


Figure 16. Sample faces of MIT database images a) Host face b) Target faces

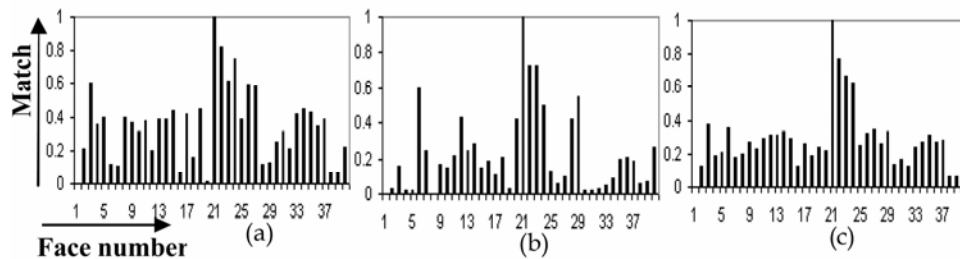


Figure 17. Match between host face and training faces on feature sets a) Geometric b) Geometric-Gabor c) Extended-Geometric

The comparison of the present method with the well known algorithms for face recognition such as eigenface (Turk and Pentland 1991) and elastic graph matching (Wiskott et al. 1999) with respect to the recognition performance is presented in the Table 7.

Method	Face Databases	
	MIT	ORL
Eigenface (Turk 1991)	97%	80 %
Elastic graph Matching (Wiskott 1999)	97%	80 %
Fuzzy face model with optimized feature set (Hiremath and Danti, Sept. 2005)	89 %	91 %

Table 7. Recognition Performance

The eigenface method did reasonably better on MIT database with 97% recognition and also has acceptable performance on ORL database with 80% recognition. Eigenface technique uses minimum Euclidian distance classifier, which is optimal in performance only if the lighting variation between training and testing images is around zero-mean. Otherwise, minimum distance classifier deviates significantly from the optimal performance, which is resulting in the deterioration of performance. Elastic matching method also performed well on the MIT database with 97% recognition and 80% recognition on ORL database. This method utilizes Gabor features covering entire face and it has some disadvantages due to their matching complexity, manual localization of training graphs and overall execution time.

The present method performed reasonably well on MIT database with 89% recognition, which is comparable to the other two methods, and has significantly improved performance on ORL database with 91% recognition. The comparison reveals that the Extended-Geometric feature vector is more discriminating and easy to discern from others and has a credit of low dimensional feature vector when compared to the high dimensional vectors used in other two methods. The reduced dimension has increased the recognition speed significantly a reduced the computation cost considerably.

## 5. Symbolic Data Approaches for Face Recognition

The symbolic data analysis (SDA) is an extension of classical data analysis to represent more complex data. Features characterizing symbolic object may be large in number, which leads to creation of a multi-dimensional feature space. Larger the dimensionality, more severe is the problem of storage and analysis. Hence, a lot of importance has been attributed to the process of dimensionality or feature reduction of symbolic objects, which is achieved by sub setting or transformation methods. Nagabhushan et. al. proposed the dimensionality reduction method on interval data based on Taylor series (Nagabhushan et. al. 1995). Ichino (Ichino 1994) proposed an extension of a PCA based on a generalized Minkowski metrics in order to deal with interval, set valued structure data. Choukria, Diday and Cazes (Choukria et. al. 1995) proposed different methods, namely, Vertices Method (V-PCA), Centers Method and Range Transformation Method. The idea of using kernel methods has also been adopted in the Support Vector Machines (SVM) in which kernel functions replace the nonlinear projection functions such that an optimal separating hyperplane can be constructed efficiently (Bozer et. al. 1992). Scholkopf et. al. proposed the use of kernel PCA for object recognition in which the principal components of an object image comprise a feature vector to train a SVM (Scholkopf et al. 1998). Empirical results on character recognition using MNIST data set and object recognition using MPI chair database show that kernel PCA is able to extract nonlinear features. Yang et al., compared face recognition performance using kernel PCA and the eigenfaces method (Yang et al. 2000). Moghaddam demonstrated that

kernel PCA performed better than PCA for face Recognition (Moghaddam 2002). Chengjun Liu extended kernel PCA method to include fractional power polynomial models for enhanced face recognition performance. (Chengjun Liu 2004). In (Hiremath and Prabhakar, 2006), an integrated approach based on symbolic data analysis and kernel PCA for face recognition is explored.

### 5.1 Symbolic Kernel PCA for Face Recognition

This section details the face recognition method using symbolic kernel PCA method (Hiremath and Prabhakar, 2006). In the training phase, firstly, the symbolic faces are constructed for a given face database images. Secondly, symbolic kernel PCA is applied to the symbolic faces in order to nonlinearly derive low dimensional interval type features that incorporate higher order statistics. In the classification phase, the test symbolic face is constructed for a given test face class in order to derive the symbolic kernel PCA interval-type features. Finally, a minimum distance classifier is employed for classification using appropriate symbolic dissimilarity measure.

#### Construction of Symbolic Faces

Consider the face images  $\Gamma_1, \Gamma_2, \dots, \Gamma_n$ , each of size  $N \times M$ , from a face image database. Let  $\Omega = \{\Gamma_1, \dots, \Gamma_n\}$  be the collection of  $n$  face images of the database, which are first order objects. Each object  $\Gamma_l \in \Omega$ ,  $l=1, \dots, n$ , is described by a feature vector  $(\tilde{Y}_1, \dots, \tilde{Y}_p)$ , of length  $p = NM$ , where each component  $\tilde{Y}_j$ ,  $j=1, \dots, p$ , is a single valued variable representing the intensity values of the face image  $\Gamma_l$ . An image set is a collection of face images of  $m$  different subjects and each subject has different images with varying expressions, orientations and illuminations. The face images are arranged from right side view to left side view. Thus there are  $m$  number of second order objects (face classes) denoted by  $F = \{c_1, c_2, \dots, c_m\}$ , each consisting of different individual images,  $\Gamma_l \in \Omega$ , of a subject. The view range of each face class is partitioned into  $q$  sub face classes and each sub face class contains  $r$  number of images. The feature vector of  $k^{th}$  sub face class  $c_i^k$  of  $i^{th}$  face class  $c_i$ , where  $k=1, 2, \dots, q$ , is described by a vector of  $p$  interval variables  $Y_1, \dots, Y_p$ , and is of length  $p = NM$ . The interval variable  $Y_j$  of  $k^{th}$  sub face class  $c_i^k$  of  $i^{th}$  face class is described as:

$$Y_j(c_i^k) = [x_{ij}^k, \bar{x}_{ij}^k] \quad (40)$$

where  $x_{ij}^k$  and  $\bar{x}_{ij}^k$  are minimum and maximum intensity values, respectively, among  $j^{th}$  pixels of all the images of sub face class  $c_i^k$ . This interval incorporates variability of  $j^{th}$  feature inside the  $k^{th}$  sub face class  $c_i^k$ .

$$\text{We denote, } X_i^k = (Y_1(c_i^k), \dots, Y_p(c_i^k)), i=1, \dots, m, k=1, \dots, q. \quad (41)$$

The vector  $X_i^k$  of interval variables is recorded for  $k^{th}$  sub face class  $c_i^k$  of  $i^{th}$  face class. This vector is called as *symbolic face* and is represented as:

$$X_i^k = (\alpha_{i1}^k, \dots, \alpha_{ip}^k) \quad (42)$$

where  $\alpha_{ij}^k = Y_j(c_i^k) = [\underline{x}_{ij}^k, \overline{x}_{ij}^k]$ ,  $j=1, \dots, p$  and  $k=1, \dots, q$ ;  $i=1, 2, \dots, m$ . We represent the  $qm$  symbolic faces by a  $(qm \times p)$  matrix  $\underline{X}$  consisting of  $qm$  row vectors  $X_i^k$  :

$$\underline{X} = \left[ X_i^k \right]_{qm \times p} \quad (43)$$

#### Extraction of Non Linear Interval Type Features

Let us consider the matrix  $\underline{X}$  containing  $qm$  symbolic faces pertaining to the given set  $\Omega$  of images belonging to  $m$  face classes. The centers  $x_{ij}^{kC} \in \mathfrak{R}$  of the intervals  $\alpha_{ij}^k = [\underline{x}_{ij}^k, \overline{x}_{ij}^k]$ , are given by

$$x_{ij}^{kC} = \frac{\overline{x}_{ij}^k + \underline{x}_{ij}^k}{2}, \text{ where } k=1, \dots, q, \quad i=1, \dots, m \text{ and } j=1, \dots, p. \quad (44)$$

The  $qm \times p$  data matrix  $\underline{X}^C$  containing the centers  $x_{ij}^{kC} \in \mathfrak{R}$  of the intervals  $\alpha_{ij}^k$  for  $qm$  symbolic faces is given by:

$$\underline{X}^C = \left[ X_i^{kC} \right]_{qm \times p} \quad (45)$$

Where the  $p$ -dimensional vectors  $X_i^{kC} = (x_{i1}^{kC}, \dots, x_{ip}^{kC})$ ,  $\underline{X}_i^k = (\underline{x}_{i1}^k, \dots, \underline{x}_{ip}^k)$  and  $\overline{X}_i^k = (\overline{x}_{i1}^k, \dots, \overline{x}_{ip}^k)$  represent the centers, lower bounds and upper bounds of the  $qm$  symbolic faces  $X_i^k$ , respectively. Let  $\Phi: \mathfrak{R}^p \rightarrow F$  be a nonlinear mapping between the input space and the feature space. For kernel PCA, the nonlinear mapping,  $\Phi$ , usually defines a kernel function. Let  $D$  represent the data matrix of centers of  $qm$  symbolic faces in the feature space:  $D = [\Phi(X_1^1C), \dots, \Phi(X_1^qC), \dots, \Phi(X_m^1C), \dots, \Phi(X_m^qC)]$ . Let  $K \in \mathfrak{R}^{qm \times qm}$  define a kernel matrix by means of dot product in the feature space:

$$K_{ij} = (\Phi(X_i) \cdot \Phi(X_j)) \quad (46)$$

Assume the mapped data is centered. As described in (Scholkopf et al., 1998), the eigenvalues,  $\lambda_1 \geq \lambda_2 \geq \dots \geq \lambda_{qm}$ , and the eigenvectors  $V_1, V_2, \dots, V_{qm}$ , of kernel matrix  $K$  can be derived by solving the following equation:

$$KA = qm\Lambda A, \text{ with } A = [a_1, \dots, a_{qm}], \quad \Lambda = \text{diag}\{\lambda_1, \dots, \lambda_{qm}\} \quad (47)$$

where  $A \in \mathfrak{R}^{qm \times qm}$  is an orthogonal eigenvector matrix,  $\Lambda \in \mathfrak{R}^{qm \times qm}$  a diagonal eigen value matrix with diagonal elements in decreasing order. In order to derive the eigenvector matrix  $V = [V_1, V_2, \dots, V_{qm}]$  of symbolic kernel PCA, first,  $A$  should be normalized such that  $\lambda_u \|a_u\|^2 = 1, u = 1, \dots, qm$ . The eigenvector matrix,  $V$ , is then derived as follows:

$$V = D^T A \quad (48)$$

A subspace is extracted from the  $p \times qm$  dimensional space  $V$  by selecting  $S \leq qm$  number of eigenvectors, which contain maximum variance and are denoted by  $V_1, V_2, \dots, V_S$ , corresponding to eigenvalues  $\lambda_1 \geq \lambda_2 \geq \dots \geq \lambda_S$ . The  $v^{th}$  eigenvector of  $V$  is denoted by  $V_v = (V_{v1}, \dots, V_{vp})$ . Since, the symbolic face  $X_i^k$  is located between the lower bound symbolic face  $\underline{X}_i^k$  and upper bound symbolic face  $\bar{X}_i^k$ , it is possible to find  $v^{th}$  interval principal component  $[\underline{W}_{iv}^k, \bar{W}_{iv}^k]$  of symbolic face  $X_i^k$  defined by

$$\underline{W}_{iv}^k = \sum_{j:V_{vj}<0} \left( \Phi(\bar{x}_{ij}^k) - \overline{\Phi(x_{ij}^k)} \right) \cdot V_{vj} + \sum_{j:V_{vj}>0} \left( \Phi(\underline{x}_{ij}^k) - \overline{\Phi(x_{ij}^k)} \right) \cdot V_{vj} \quad (49)$$

$$\bar{W}_{iv}^k = \sum_{j:V_{vj}<0} \left( \Phi(\underline{x}_{ij}^k) - \overline{\Phi(x_{ij}^k)} \right) \cdot V_{vj} + \sum_{j:V_{vj}>0} \left( \Phi(\bar{x}_{ij}^k) - \overline{\Phi(x_{ij}^k)} \right) \cdot V_{vj} \quad (50)$$

where  $v = 1, \dots, S$ , and  $\overline{\Phi(x_{ij}^k)} = \left[ \sum_{i,j} \Phi(x_{ij}^k) \right] / qm$ . Let  $c_{test}$  be the test face class, which contains face images of same subject with different expression, lighting condition and orientation. The test face class  $C_{test}$  is described by a feature vector  $X_{test}$  termed as test symbolic face of  $p$  interval variables  $Y_1, \dots, Y_p$ , and is of length  $p = NM$ . The interval variable  $Y_j$  of test symbolic face is described as  $Y_j(X_{test}) = [\underline{x}_{(test)j}, \bar{x}_{(test)j}]$ , where  $\underline{x}_{(test)j}$ , and  $\bar{x}_{(test)j}$  are minimum and maximum intensity values, respectively, among  $j^{th}$  pixels of all the images of test face class  $c_{test}$ . This interval incorporates information of the variability of  $j^{th}$  feature inside the test face class  $C_{test}$ . The lower bound of test symbolic face  $X_{test}$  is described as  $\underline{X}_{(test)} = (\underline{x}_{(test)1}, \underline{x}_{(test)2}, \dots, \underline{x}_{(test)p})$ . Similarly, the upper bound is described as  $\bar{X}_{(test)} = (\bar{x}_{(test)1}, \bar{x}_{(test)2}, \dots, \bar{x}_{(test)p})$ . The  $v^{th}$  interval principal component  $[\underline{W}_{(test)v}, \bar{W}_{(test)v}]$  of test symbolic face  $X_{test}$  is computed as:

$$\underline{W}_{(test)v} = \sum_{j:V_{vj}<0} \left( \Phi(\bar{x}_{(test)j}) - \overline{\Phi(x_{(test)j}^C)} \right) \cdot V_{vj} + \sum_{j:V_{vj}>0} \left( \Phi(\underline{x}_{(test)j}) - \overline{\Phi(x_{(test)j}^C)} \right) \cdot V_{vj} \quad (51)$$

$$\bar{W}_{(test)v} = \sum_{j:V_{vj}<0} \left( \Phi(\underline{x}_{(test)j}) - \overline{\Phi(x_{(test)j}^C)} \right) \cdot V_{vj} + \sum_{j:V_{vj}>0} \left( \Phi(\bar{x}_{(test)j}) - \overline{\Phi(x_{(test)j}^C)} \right) \cdot V_{vj} \quad (52)$$

where  $v = 1, \dots, S$ , and  $\overline{\Phi(x_{(test)j}^C)} = \frac{\bar{x}_{(test)j} + \underline{x}_{(test)j}}{2}$ .

## 5.2 Classification Rule

When test face class  $C_{test}$  is presented to the symbolic kernel PCA classifier, low dimensional symbolic kernel PCA interval type features  $[\underline{W}_{(test)v}, \bar{W}_{(test)v}]$  are derived. Let  $[\underline{W}_{iv}^k, \bar{W}_{iv}^k]$ ,  $i=1, 2, \dots, m$ , and  $k=1, \dots, q$ , be the symbolic kernel PCA interval type features of  $qm$  symbolic

faces. The classifier applies the minimum distance rule for classification using symbolic dissimilarity measure  $\delta$ :

$$\delta\left([\underline{W}_{(test)v}, \overline{W}_{(test)v}], [\underline{W}_{iv}^k, \overline{W}_{iv}^k]\right) = \min_i \delta\left([\underline{W}_{(test)v}, \overline{W}_{(test)v}], [\underline{W}_{iv}^k, \overline{W}_{iv}^k]\right) \rightarrow c_{test} \in c_i \quad (53)$$

The symbolic kernel PCA interval type feature vector  $[\underline{W}_{(test)v}, \overline{W}_{(test)v}]$  is classified as belonging to the face class,  $c_i$ , using appropriate symbolic dissimilarity measure  $\delta$ . Two classes of kernel functions widely used in kernel classifiers are polynomial kernels and Gaussian kernels defined, respectively, as:

$$k(x, y) = (x \cdot y)^d \quad (54)$$

$$k(x, y) = \exp\left(-\frac{\|x - y\|^2}{2\sigma^2}\right), \text{ where } d \in \mathbb{N}, \sigma > 0 \text{ and } k > 0. \quad (55)$$

### 5.3 Experimental Results

The symbolic kernel PCA method is experimented with the face images of the ORL face database, which composed of 400 images with ten different images for each of the 40 distinct subjects. All the images were taken against a dark homogeneous background with the subjects in an upright, frontal position, with tolerance for some tilting and rotation of up to about  $20^\circ$  from frontal view to left side view and right side view. In the training phase, each face class is partitioned into three sub face classes based on view range from right side view to left side view. Each sub face class will have three images and totally nine images of one subject are used for training purpose. Thus, we obtain the 120 symbolic faces. The symbolic kernel PCA is applied to obtain the non-linear interval type features from symbolic faces. The classification phase includes construction of test symbolic face for each trial using randomly selected three images from each face class and extraction of interval type features from test symbolic face. Further, a minimum distance classifier is employed for classification using symbolic dissimilarity measure. Figure 18(a) shows some typical images of one subject of ORL database and their corresponding view based arrangement. Figure 18(b) shows the constructed symbolic faces for face class shown in (a).



Figure 18. (a) Arrangement of faces images from right to left side view belonging to one subject of ORL database. (b) Three symbolic faces of face class shown in (a) and each symbolic face summarizes the variation of feature values through the images belonging to corresponding sub face class (each interval of symbolic face is centered for display purpose)

### Performance of symbolic kernel PCA using symbolic dissimilarity measures

Experimentation is done to compare performance of symbolic kernel PCA with polynomial kernel of degree one using symbolic dissimilarity measures. The recognition accuracy (%) of 64.50, 71.25 and 78.15 is observed in the experiments using symbolic dissimilarity measures (Bock & Diday 2000): Gowda and Diday, Ichino and Yaguchi and De Carvalho and Diday dissimilarity measures, respectively. Hence, De Carvalho and Diday dissimilarity measure is considered appropriate for face recognition using symbolic kernel PCA method.

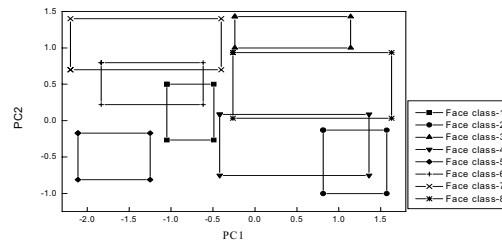


Figure 19. Rectangular representation of first two principal components of eight face classes

### Performance of symbolic kernel PCA with varying number of features

Two popular kernels are used in the experimentation. One is the polynomial kernel (equation 5.15) and the other is Gaussian kernel (equation 5.16). Three methods, namely, conventional kernel PCA, eigenface method and symbolic kernel PCA method, are tested and compared. The minimum distance classifier is employed in the experiments. In the phase of model selection, the goal is to determine proper kernel parameters (i.e., the order  $d$  of the polynomial kernel and the width  $\sigma$  of the Gaussian kernel), the dimension of the projection subspace for each method. Since it is very difficult to determine these parameters, a stepwise selection strategy is adopted here. Specifically one has to fix the dimension and try to find the optimal kernel parameters for a given kernel function. Then, based on the chosen kernel parameters, the selection of the subspace sizes is performed. To determine the proper parameters for kernels, we use the global to local strategy. After globally searching over a wide range of the parameter space, we find a candidate interval where the optimal parameters might exist. Here, for the polynomial kernel, the candidate order interval is from 1 to 7 and, for the Gaussian kernel, the candidate width interval is from 0.5 to 12. Then, we try to find the optimal kernel parameters within these intervals. Figure 20 (a) and (b) show the recognition accuracy versus the variation of kernel parameters corresponding to conventional kernel PCA, and symbolic kernel PCA method with a fixed dimension of 30. From these figures, the optimal order of polynomial kernel is found to be three and the width of Gaussian kernel should be five for symbolic kernel PCA method. After determining the optimal kernel parameters, we set out to select the dimension of subspace.

Method	Polynomial Kernel		Gaussian Kernel	
	Order	Subspace Dimension	Width	Subspace Dimension
Conventional Kernel PCA	1	44	7	47
Symbolic Kernel PCA	3	35	5	44

Table 8. Optimal Parameters corresponding to each method with respect to two different kernels

We depict the performance of each method over the variation of dimensions and present them in Figure 20(c) and (d). From these figures, the optimal subspace dimension can be chosen for each method with respect to different kernels. The optimal parameters for each method with respect to different kernels are listed in Table 8. After selection of optimal parameters for each method with respect to different kernels, all three methods are reevaluated using same set of training and testing samples. The number of features and recognition accuracy for the best case are shown in Table 9. The best performance of the symbolic kernel PCA method is better than the best performance of the conventional kernel PCA and eigenface method. We note that the symbolic kernel PCA method outperforms eigenface method and conventional kernel PCA in the sense of using small number of features. This is due to the fact that first few eigenvectors of symbolic kernel PCA method account for highest variance of training samples and these few eigenvectors are enough to represent image for recognition purposes. Hence, improved recognition results can be achieved at less computational cost by using symbolic kernel PCA method, by virtue of its low dimensionality.

	Eigenface	Symbolic Kernel PCA		Conventional Kernel PCA	
		Polynomial Kernel	Gaussian Kernel	Polynomial Kernel	Gaussian Kernel
Recognition Rate (%)	78.11	91.15	90.25	84.95	81.35
Number of Features	47	35	44	44	47

Table 9. Comparison of symbolic kernel PCA Method using optimal parameters

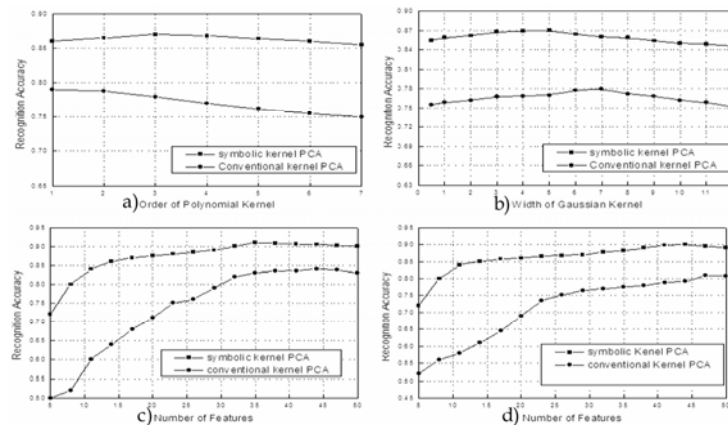


Figure 20. Illustration of recognition rates over the variations of kernel parameters and subspace dimensions. a) order of polynomial kernel b) Width of Gaussian kernel c) Subspace dimension using polynomial kernel with optimal order d) Gaussian kernel with optimal width

The symbolic kernel PCA method is also superior in terms of computational efficiency for feature extraction. In the Table 10, CPU times (in seconds) required for feature extraction by different methods are presented. It is observed that the symbolic kernel PCA method is found to be faster.

Eigenface	Symbolic Kernel PCA		Conventional Kernel PCA	
	Polynomial Kernel	Gaussian Kernel	Polynomial Kernel	Gaussian Kernel
124	78	116	91	131

(CPU: Pentium 2.5GHz, RAM: 248 MB)

Table 10. The CPU Time(s) for feature extraction corresponding to each method

## 6. Symbolic Factorial Discriminant Analysis for Face Recognition

In the framework of symbolic data analysis (SDA), a generalization of the classical factorial discriminant analysis to symbolic objects is proposed in (Hiremath and Prabhakar, Sept. 2006), which is termed as symbolic factorial discriminant analysis (symbolic FDA). It consists of a symbolic-numerical-symbolic procedure for face recognition under variable lighting. In the first phase, the face images are represented as symbolic objects of interval type variables. The representation of a face images as symbolic faces results in coverage of image variations of human faces under different lighting conditions and also enormously reduces the dimension of the original image space without losing a significant amount of information. Symbolic FDA proceeds by a numerical transformation of the symbolic faces, using a suitable coding. Optimal quantification step of the coded variables is achieved by Non-Symmetrical Multiple Correspondence Analysis (NS-MCA) proposed by Verde and Lauro. This yields new factorial variables, which will be used as predictors in the analysis. In the second phase, we applied symbolic factorial discriminant analysis method on the centered factorial variables to extract interval type discriminating features, which are robust to variations due to illumination. This procedure is detailed as given below.

### 6.1 Construction of symbolic Faces

We construct the  $qm$  symbolic faces by a matrix  $E$  with size  $(qm \times p)$ , consisting of row vectors  $S_i^k = (Y_1(c_i^k), \dots, Y_p(c_i^k))$ ,  $i = 1, \dots, m$ ,  $k = 1, \dots, q$ , as described in the section 5.1. The  $p$ -dimensional vectors,  $\underline{S}_i^k = (x_{i1}^k, \dots, x_{ip}^k)$  and  $\overline{S}_i^k = (\overline{x}_{i1}^k, \dots, \overline{x}_{ip}^k)$  represent the lower bounds and upper bounds of the symbolic face  $S_i^k$ , respectively.

#### Coding of Symbolic Variables

This phase performs a numerical transformation of the interval variables by means of dichotomic and non-linear functions. The coding values are collected in coding matrices that we denote by  $X_j$  ( $j = 1, \dots, p$ ). We adopt a fuzzy coding system in order to preserve as much as possible the numerical information of the original variables after their categorization. For this purpose, a interval type variable is transformed based on a fuzzy approach using special piece wise polynomial functions, such as *B-Splines*, as has been proposed by Van Rijeckevorsel and Verde (Bock & Diday 2000). In order to attain a reasonably small number of categories for the coded variables, typically low degree polynomials are used. By a B-Spline of degree one, or a semi linear transformation, the domain of each variable is split into two intervals and a fuzzy coding is performed by three semi linear functions, e.g.  $B_1, B_2, B_3$ . The threshold knots are chosen as the minimum and maximum values assumed by the variable and middle knot might be the average, median, or the semi range value of the variable. According to the B-Spline coding system, a symbolic face  $S_i^k$  is coded as a unique

row in the matrix  $X_j$  corresponding to the values assumed by the B-Spline functions for the value  $Y_j$  for a  $S_i^k : B_1(Y_j(S_i^k)), B_2(Y_j(S_i^k)), B_3(Y_j(S_i^k))$ . Finally, a global coding matrix  $X_{N \times K}$  is constructed by combining coded descriptors. It is also considered as a partitioned matrix built by juxtaposing  $p$  fuzzy coding matrices obtained in coding phase:

$$X = \left[ \left[ X_1 \mid \cdots \mid X_j \mid \cdots \mid X_p \right] \right] \quad (56)$$

here  $K = 3g$ , ( $g \leq p$ ) is the number of columns of  $X_j$  of all transformed variables in the descriptions of the symbolic faces. The total number  $N$  of rows of  $X$  will be larger than the original number  $qm$  of symbolic faces.

#### Quantification of symbolic variables

After the coding of the variables in terms of fuzzy coding, we want to find a quantification of the coded variables. The optimal quantification of the  $K$  categories of the  $p$  descriptors is obtained as solution of the eigen equation:

$$\frac{1}{N} \left( G' X \Delta_x^{-1} X' G - \frac{n}{N} G' U G \right) \omega_\alpha = \mu_\alpha \omega_\alpha \quad (57)$$

where  $G_{N \times qm}$  be the indicator matrix that identifies the different symbolic faces of the set  $E$ . Under the ortho-normality constraints:  $w'_\alpha w_\alpha = 1$  and  $w'_\alpha w_{\alpha'} = 0$  for  $\alpha \neq \alpha'$ . Here  $U$  is a matrix with unitary elements,  $\mu_\alpha$  and  $\omega_\alpha$  are the  $\alpha^{\text{th}}$  eigen value and eigenvector, respectively, of the matrix in the brackets, and  $\Delta_x^{-1}$  is the block diagonal matrix with diagonal blocks  $(X'_j X_j)^{-1}$ . New quantified variables associated with the  $\alpha^{\text{th}}$  factorial axis is computed as:

$$\Phi_\alpha = X \Delta_x^{-1} X' G \omega_\alpha \in \mathfrak{R}^N \quad (58)$$

#### Extraction of Interval Type Features

After having transformed the categorical predictors into optimal numerical variables, we can perform a classical FDA in order to look for a suitable subspace with optimum separation and, at the same time, obtaining a minimum internal dispersion of the corresponding symbolic faces. We denote by  $\tilde{X}$  matrix collecting the new variables  $|\Phi_1| \cdots |\Phi_\alpha| \cdots |\Phi_s|$  of set  $E$ . The factorial discriminant axes are solutions of the eigen equation:

$$\left[ \left( \tilde{X}' H \tilde{X} \right)^{-1} \left( \tilde{X}' H C \right) \left( C' H C \right)^{-1} \left( C' H \tilde{X} \right) \right] y_\alpha = \lambda_\alpha y_\alpha \quad (59)$$

where the column vectors of  $\tilde{X}$  are centered, and  $C$  is the indicator matrix that specifies the membership of each symbolic face to just one of the  $m$  classes  $c_i$ . Here  $H$  is the diagonal matrix with diagonal elements equal to  $d_i/qm$  ( $i = 1, \dots, m$ ), where  $d_i$  are the class sizes, and  $\lambda_\alpha$  and  $y_\alpha$  are the  $\alpha^{\text{th}}$  eigen value and eigenvector, respectively, of the matrix in brackets. The eigenvectors of symbolic factorial discriminant analysis method can be obtained as:

$$V_{qm} = E' Y_{qm} \quad (60)$$

where  $V_{qm}=(v_1, \dots, v_{qm})$  is the  $qm \times qm$  matrix with columns  $v_1, \dots, v_{qm}$  and  $Y_{qm}$  is the  $P \times qm$  matrix with corresponding eigenvectors  $y_1, y_2, \dots, y_{qm}$ , as its columns. The  $\alpha^{th}$  eigenvector of  $V$  is denoted by  $v_\alpha=(v_{\alpha 1}, \dots, v_{\alpha p})$ . A subspace is extracted by selecting  $L$  number of eigenvectors, which contain maximum variance and are denoted by  $v_1, v_2, \dots, v_L$ , corresponding to eigenvalues  $\lambda_1 \geq \lambda_2 \geq \dots \geq \lambda_L$ . Since, the symbolic face  $S_i^k$  is located between the lower bound symbolic face  $\underline{S}_i^k$  and upper bound symbolic face  $\overline{S}_i^k$ , it is possible to find  $\alpha^{th}$  interval principal component  $[\underline{W}_{i\alpha}^k, \overline{W}_{i\alpha}^k]$  of symbolic face  $S_i^k$  defined by

$$\underline{W}_{i\alpha}^k = \underline{S}_i^k v_\alpha \quad (61)$$

$$\overline{W}_{i\alpha}^k = \overline{S}_i^k v_\alpha \quad (62)$$

## 6.2 Classification of Rule

Let  $c_{test}$  be the test face class, which contains face images of same subject under varying illumination conditions. The test symbolic face  $S_{test}$  is constructed for test face class  $c_{test}$ . The lower bound of test symbolic face  $S_{test}$  is described as  $\underline{S}_{(test)} = (\underline{x}_{(test)1}, \underline{x}_{(test)2}, \dots, \underline{x}_{(test)p})$ . Similarly, the upper bound is described as  $\overline{S}_{test} = (\overline{x}_{(test)1}, \overline{x}_{(test)2}, \dots, \overline{x}_{(test)p})$ . A matrix representation for the test symbolic face is obtained by the same coding system and the coded descriptors are collected in a global coding matrix  $X^+ = (X_1^+ | \dots | X_p^+)$  of dimension  $(N^+, K)$ . The quantification of the coded descriptors of test symbolic face is achieved by:

$$\Phi_\alpha^+ = X^+ \Delta_x^{-1} X' G \omega_\alpha \quad (63)$$

where  $\omega_\alpha$  are the eigenvectors obtained as solutions of the equation (57). The  $\alpha^{th}$  interval principal component  $[\underline{W}_{(test)\alpha}, \overline{W}_{(test)\alpha}]$  of test symbolic face  $S_{test}$  is computed as:

$$\underline{W}_{(test)\alpha} = \underline{S}_{test} v_\alpha \quad (64)$$

$$\overline{W}_{(test)\alpha} = \overline{S}_{test} v_\alpha \quad (65)$$

Let  $[\underline{W}_{i\alpha}^k, \overline{W}_{i\alpha}^k]$ ,  $i=1, 2, \dots, m$ , and  $k=1, \dots, q$ , be the interval type features of  $qm$  symbolic faces. The classifier applies the minimum distance rule for classification using De Carvalho and Diday symbolic dissimilarity measure  $\delta$  (Bock & Diday 2000).

$$\delta \left( [\underline{W}_{(test)\alpha}, \overline{W}_{(test)\alpha}], [\underline{W}_{i\alpha}^k, \overline{W}_{i\alpha}^k] \right) = \min_i \delta \left( [\underline{W}_{(test)\alpha}, \overline{W}_{(test)\alpha}], [\underline{W}_{i\alpha}^k, \overline{W}_{i\alpha}^k] \right) \quad (66)$$

$\rightarrow c_{test} \in c_i$

The interval type feature vector  $[\underline{W}_{(test)\alpha}, \overline{W}_{(test)\alpha}]$  is classified as belonging to the face class,  $c_i$ , using De Carvalho and Diday symbolic dissimilarity measure  $\delta$ .

### 6.3 Experimental Results

In order to demonstrate the effectiveness of symbolic factorial discriminant analysis method for face recognition under varying illumination conditions, we have conducted a number of experiments by using 4,050 image subset of the publicly available Yale Face Database B (Georghiadis et. al. 2001). This subset contains 405 viewing conditions of 10 individuals in 9 poses acquired under 45 different point light sources and an ambient light. The pose variation is limited to only upto  $10^\circ - 15^\circ$ . The images from each pose were divided into four subsets ( $12^\circ, 25^\circ, 50^\circ$  and  $77^\circ$ ) according to the angle  $\theta$  between the direction of the light source and the optical axis of a camera. Subset 1 (respectively 2, 3, 4) contains 70 (respectively 120, 120, 140) images per pose. In the experiments, images which were cropped and down-sampled to  $64 \times 64$  pixels by averaging are used. Actually, in order to remove any bias due to the scale and position of a face in each image from the recognition performance, they were aligned so that the locations of the eyes or the face center were the same. In Figure 21, we show images of an individual belonging to each subset. One can confirm that images vary significantly depending on the direction of the light source.



Figure 21. Images of an individual belonging to each subset: the angle  $\theta$  between the light source direction and the optical axis lie  $(0^\circ, 12^\circ)$ ,  $(20^\circ, 25^\circ)$ ,  $(35^\circ, 52^\circ)$  and  $(60^\circ, 77^\circ)$  respectively

We have conducted several experiments to compare our algorithm with two other algorithms. In particular, we compared our algorithm with eigenfaces (Turk & Pentlad 1991) and kernel Fisher discriminant analysis algorithm (Yang et. al 2005). Eigenfaces is the defacto baseline standard by which face recognition algorithms are compared. In the present study, we have assumed that more probe images are available. The proposed method improves the recognition accuracy as compared to other algorithms by considering three probe images with wide variations in illuminations and pose for each trial. In all the experiments, simplest recognition scheme namely, a minimum distance classifier with symbolic dissimilarity measure is used.

#### Variations in illumination and fixed pose

The first set of face recognition experiments, where the illumination varies while pose remains fixed are conducted using 450 images (45 per face) for both training and testing. The goal of these experiments was to test the accuracy of this method. First, we used images belonging to subset 1 ( $\theta < 12^\circ$ ) as training images of each individual, and then tested other images ( $\theta \geq 20^\circ$ ).

Method	Recognition error rates (%)		
	Subset 2	Subset 3	Subset 4
Symbolic FDA	0	0	4.3
Eigenfaces	7.6	22.50	60.90
KFDA	2.5	12.45	50.8

Table 11. Comparison of recognition error rates under variations in illuminations and fixed pose

In Table 11, we show the recognition error rates of different methods for each subset. The results show that the proposed method outperforms other methods when illumination varies while pose remains fixed. This is due to the fact that the first subset allows images with maximum intensity among images of the subsets and any possible intensity values lies within intervals constructed by using subset 1.

#### Variations in illumination and pose

Secondly, the experiments are conducted by using images taken under varying illumination conditions and poses, and confirmed the robustness of symbolic FDA method against variations due to slight changes in pose. In these experiments, the images in five poses instead of images in frontal pose only are used. The criteria used to select both training set and test set are same as like previous experiments but for five poses of each individual. In Table 12, the recognition error rates of symbolic FDA method and other two methods for each subset are given. The results show that the symbolic FDA method outperforms other methods for images with variations in illuminations and pose.

Method	Recognition error rates (%)		
	Subset 2	Subset 3	Subset 4
symbolic FDA	0	0.5	5.5
Eigenfaces	3.8	15.7	25.65
KFDA	3.0	22.5	14.5

Table 12. Comparison of recognition error rates under variations in illuminations and pose

## 7. Conclusions

Face is a more common and important biometric identifier for recognizing a person in a non-invasive way. The face recognition involves identification of the facial features, namely, eyes, eyebrows, nose, mouth, ears, and their spatial interrelationships uniquely. The variability in the facial features of the same human face due to changes in facial expressions, illumination and poses shall not alter the face recognition. In the present chapter we have discussed the modeling of the uncertainty in information about facial features for face recognition under varying face expressions, poses and illuminations. There are two approaches, namely, fuzzy face model based on fuzzy geometric rules and symbolic face model based on extension of symbolic data analysis to PCA and its variants. The effectiveness of these approaches is demonstrated by the results of extensive experimentation using various face databases, namely, ORL, FERET, MIT-CMU and CIT. The fuzzy face model as well as symbolic face model are found to capture variability of facial features adequately for successful face detection and recognition.

## 8. References

- Belhumeur, P.N., Hespanha, J.P., Kriegman, D.J. (1997), Eigenfaces vs. Fisherfaces: Recognition using class specific Linear Projection, *IEEE Trans. on PAMI*, vol.19(7),711-720.
- Bock, H.H., Diday, E. (Eds.) (2000): Analysis of Symbolic Data. *Springer Verlag*.
- Bojic, N., and Pang, K.K., 2000, Adaptive skin segmentation for head and shoulder video sequence, *SPIE VCIP'2000*, Perth, Australia

- Bozer, Guyon, Vapnik, (1992). A training algorithm for optimal margin classifiers. In *Proc. of workshop on Computational Learning Theory*, 144-152.
- Brunelli, R., and Poggio, T., (1993), Face recognition: Features versus Templates, *IEEE Trans. Pattern Analysis and Mach. Intell.* Vol.15, pp.1042-1052
- Chai, D., and Ngan, K.N., (1999), Face segmentation using skin color map in videophone applications, *IEEE Trans. CSVT*, Vol. 9(4), pp. 551-564
- Chellappa, R., Wilson, C.L., Sirohey, S., (1995). Human and Machine Recognition of Faces: A Survey. *Proc. IEEE* 83 (5), 704-740.
- Chengjun Liu, (2004) . Gabor Based Kernel PCA with Fractional Power Polynomial Models for Face Recognition, *IEEE Trans. PAMI*, vol-26, 572-581.
- Choukria, Diday, Cazes (1995). Extension of the principal component analysis to interval data. Presented at *NTTS'95: New Techniques and Technologies for statistics*, Bonn
- Diday, (1993). An introduction to symbolic data analysis. Tutorial at *IV Conf. IFCS*.
- Daugman, J.D., (1980), Two dimensional spectral analysis of cortical receptive field profiles, *Vision Research*, Vol. 20, 847-856
- Duc, B., Fisher, S., and Bigün, J., (1999), Face Authentication with Gabor Information on Deformable Graphs, *IEEE Transactions on Image Proc.*, vol. 8(4), 504-515.
- Phillips, P.J., Wechsler, H., Huang, J., and Rauss, P., (1998). The FERET database and evaluation procedure for face recognition algorithms, *Image and Vision Computing*, 16, 295-306, <http://www.nist.gov/humanid/feret>
- Gabor, D., (1946), *Theory of Communications, Jr. of Inst. of Electrical Eng.*, Vol.93, pp.429-557
- Georghiades, A.S., P.N. Belhumeur, and D.J. Kriegman, (2001). From Few to Many: Illumination Cone Models for Face Recognition under Variable Lighting and Pose, *IEEE Trans. on PAMI*, 23(6): p. 643-660.
- Gonzalez R.C., Richard E., Woods. (2002). *Digital Image Processing*, Pearson Edu. 2<sup>nd</sup> Ed.
- Gowda, Diday, (1991). Symbolic clustering using a new dissimilarity measure. *Pattern Recognition*, 24(6)
- He, X., Yan, S., Hu, Y., Niyogi, P., and Zhang, H-J., (March 2005), Face Recognition Using Laplacianfaces, *IEEE transactions on PAMI*, vol. 27(3), pp. 328-340
- Hines, W.W., Douglas, C.M., (1990), *Probability and statistics in Engineering and Management Science*, John Wiley and Sons, 3<sup>rd</sup> Ed
- Hiremath, P.S., and Ajit Danti, (Feb 2006), Detection of multiple faces in an image using skin color information and Lines-of-Separability face model, *International Journal of Pattern Recognition and Artificial Intelligence*, Vol. 20(1), pp.39-69. World Scientific Publisher. (ISSN:0218-0014)
- Hiremath, P.S., and Ajit Danti, (Jan 2006), Combining geometric and Gabor features for face recognition, *Proceedings of the 7<sup>th</sup> Asian Conference on Computer Vision (ACCV-06, International Institute of Information Technology (IIIT), Hyderabad, India*, pp. 140-149, Springer Verlag Publisher (LNCS 3851, ISBN 3-540-31219-6)
- Hiremath, P.S., and Ajit Danti, (Dec 2005), Detection of Multiple Faces Based on Facial Features Using Fuzzy Face Model, *Proceedings of the International Conference on Cognition and Recognition, COGREC-05*, University of Mysore, Mysore, India, Allied Publisher (ISBN: 81-7764), pp.793-800.
- Hiremath, P.S., and Ajit Danti, (Sept. 2005), Invariant geometrical feature vector for Face recognition, *Vijnana Ganga, Journal of Science and Technology*, Gulbarga University, Vol. 4, pp.64-72. (Silver Jubilee Special Issue)

- Hiremath, P.S., and Ajit Danti, (March, 2005), A fuzzy rule based method for human face detection, *Proceedings of National Conference on Vision, Graphics and Image Processing*, Shimoga, India, 374-381
- Hiremath, P.S., and Ajit Danti, (Dec. 2004), Optimized Geometrical Feature Vector for Face Recognition, *Proceedings of the International Conference on Human Machine Interface*, Indian Institute of Science, Bangalore, pp.309-320, Tata McGraw-Hill (ISBN 0 07-059757-X)
- Hiremath, P.S., Prabhakar C.J.,(2007). Face Recognition using Symbolic KDA in the Framework of Symbolic Data Analysis, *Int. Conf. on Advances in Patt. Recog. (ICAPR2007)*, ISI, Kolkata, World Scientific, pp.56-61.
- Hiremath, P.S., Prabhakar, C.J.,(2006). Acquiring Non-linear Subspace for Face Recognition using Symbolic Kernel PCA method, *Jr. of Symbolic Data Analysis*, Vol.4(1), pp.15-26.
- Hiremath, P.S., Prabhakar, C.J. (Dec 2006). Face Recognition Technique using Symbolic Linear discriminant Analysis Method, *Proc. Of Int. Conf. on Computer Vision, Graphics and Image Processing (ICVGIP 2006)*, Springer Verlag, pp. 641-649
- Hiremath, P.S., Prabhakar, C.J. (Sept. 2006). Symbolic Factorial Discriminant Analysis for face recognition under variable lighting, *Proc. Of Int. Conf. on visual Information Engineering*, pp.26-28.
- Hiremath, P.S., Prabhakar, C.J., (Aug. 2006). Independent Component Analysis of Symbolic Data for Face Recognition, *Proc. Of Int. Conf. on Intelligent Systems and Control*, pp.255-258.
- Hiremath, P.S., Prabhakar, C.J.,(Jan 2006). Face Recognition Technique using Two-dimensional Symbolic Discriminant Analysis Algorithm, *Proc. Of 3rd workshop on Computer Vision, Graphics and Image Processing*, IIIT, Hyderabad, pp. 180-185.
- Hiremath.P.S, Prabhakar.C.J, (2005), Face Recognition Technique using Symbolic PCA Method, *Proc. Int. Conf. on Patt. Recog. & Machine Intel.* Kolkata, 266-271, Springer Verlag.
- Hsu, R.L., Abdel-Mottaleb, M., Jain, M., (2002), Face Detection in Color Images, *IEEE Trans. on Pattern Analysis and Machine Intelligence*, Vol. 24(5), pp. 696-706
- Ichino, Yaguchi (1994): Generalized Minkowski metrics for mixed feature type data analysis, vol- (4). *IEEE Trans. Systems Man Cybernet.* 698-708.
- Jain, A.K., (2001). Fundamentals of Digital Image Processing, *Prentice Hall of India Pvt. Ltd.*
- Kim, T-K., and Kittler, J., (March 2005), Locally Linear Discriminant Analysis for Multimodally Distributed Classes for Face Recognition with a Single Model Image, *IEEE trans. on PAMI*, vol. 27, no. 3, pp. 318-327
- Kirby, Sirovich (1990): Applications of the Karhunen–Loeve procedure for the characterization of human faces, v-12 (1). *IEEE Trans. PAMI.* 103-108.
- Klir, G.J., and Yuan, B., (2000), Fuzzy sets and fuzzy logic, *PHI*, Pvt Ltd, New Delhi
- Kotropoulos, C., Tefas, A., and Pitas, I., (April 2000), Frontal face authentication using morphological elastic graph matching, *IEEE Trans. Image Process.*, vol. 9(4), pp. 555–560
- Moghaddam,(2002) Principal Manifolds and Probabilistic subspaces for Visual Recognition *IEEE Trans. PAMI*, vol-19, 780-788.
- Moghaddam, B., and Pentland, A., (1997), Probabilistic visual learning for object representation, *IEEE Transaction on PAMI*, 19 (7), 696-710.

- Mohan, A., Papageorgiou, C., and Poggio, T., 2001, Example-based object detection in images by components. *IEEE Trans. PAMI*, 23(4), 349-361.
- MIT face database is available at <ftp://whitechapel.media.mit.edu/pub/images/>
- Nagabhushan, Gowda, Diday (1995): Dimensionality reduction of symbolic data, vol-16. *Pattern Recognition Letters*, 219-223.
- Olugbenga, A., Yang, Y-H., (2002), Face Recognition approach based on rank correlation of Gabor-Filtered images, *Pattern Recognition*, Vol. 35, pp. 1275-1289
- Olivetti-Oracle Research labs (ORL) face database, AT&T laboratories, Cambridge, UK <http://www.cam-orl.co.uk/facedatabase.html>
- Scholkopf and A.Smola, and K.Muller,(1998). Nonlinear Component Analysis as a kernel Eigenvalue Problem, *Neural Computation*, vol.10, pp.1299-1319
- Shan, S., Gao, W., Chang, Y., Cao, B., Yang, P., (2004), Review the strength of Gabor features for face recognition from the angle of its robustness mis-alignment, *Proceedings of the 17<sup>th</sup> International Conference on Pattern recognition (ICPR 04)*
- Shih, P. and Liu, C., (2004). Face detection using discriminating feature analysis and support vector machine in video, in *Proc. Intl. conference on Pattern recognition, Cambridge*.
- Schneiderman, H., and Kanade, T., (June 2000). A statistical model for object detection applied to faces and cars, In *Proc. IEEE Computer Society Conference on Computer Vision and Pattern Recognition*,746-751.
- Turk,M., & Pentland,A.,(1991), Eigenface for Recognition, *Jr. of Cognitive Neuroscience*, vol.3(1), pp. 71-86
- Wang, Y., and Yuan, B., (2001), A novel approach for human face detection from color images under complex background, *Pattern Recognition* Vol. 34, pp. 1983-1992
- Weber, M., Collection of color face images (CIT database) used as sample test images for experimentation and are available at the website [http://www.vision.caltech.edu/Image\\_Datasets/faces/](http://www.vision.caltech.edu/Image_Datasets/faces/)
- Wiskott, L., Fellous, J.M., Krüger N., and Christoph von der Malsburg, (1999), Face Recognition by Elastic Graph Matching, *In Intelligent Biometric Techniques in fingerprint and Face Recognition*, CRC Press, Chapter 11, pp. 355-396
- Wu, H.Q., Chen, M. Yachida, (1999). Face detection from color images using a fuzzy pattern matching method. *IEEE Trans. on Pattern Analysis and Machine Intell.* 21(6), 557-563.
- Yang, Frangi, J Y Yang, D Zhang(2005), A Complete Kernel Fisher Discriminant Framework for Feature Extraction and Recognition, *IEEE Trans. on PAMI*, v-27, 230-242.
- Yang, M.H., David J., Kriegman, Ahuja, N., (2002). Detecting Faces in Images: A Survey. *IEEE Trans. Pattern Anal. Machine Intell.* 24 (1), 34-58.
- Yang, M.H., Ahuja, N. and Kriegman, D.,(2000). Face Recognition Using Kernel Eigenfaces, *Proc. IEEE Int'l Conf. Image Processing*.
- Yao, H., and Gao, W., (2001),Face detection and location based on skin chrominance and lip chrominance transformation from color images, *Pattern recognition*, Vol. 34, pp.1555-1564
- Zhang, H., Zhang, B., Huang, W., Tian, Q., (2005), Gabor wavelet associate memory for face recognition, *IEEE Trans. on Neural Network*, Vol. 16(1), pp. 275-278
- Zhao, W., Chellappa, R., Rosenfeld, A. and Phillips, P.J., (2000), Face Recognition: A literature Survey, *CVL Technical report*, Center for automation Research, Univ. of Maryland